Mon. Not. R. Astron. Soc. **000**, 000–000 (0000) Printed 25 June 2014 (MN LATEX style file v2.2)

Clues on the Missing Sources of Reionization from Self-consistent Modeling of Milky Way and Dwarf Galaxy Globular Clusters

Harley Katz[1,2,3⋆] and Massimo Ricotti[1,4]†
[1] *Department of Astronomy, University of Maryland, College Park, MD 20742, USA*
[2] *Institute of Astronomy, University of Cambridge, Madingly Road, Cambridge, CB3 0HA, UK*
[3] *Kavli Institute for Cosmology, University of Cambridge, Madingly Road, Cambridge, CB3 0HA, UK*
[4] *Sorbonne Universits, Institut Lagrange de Paris (ILP), 98 bis Bouldevard Arago 75014 Paris, France*

arXiv:1406.6055v1 [astro-ph.GA] 23 Jun 2014

25 June 2014

ABSTRACT

Globular clusters are unique tracers of ancient star formation. We determine the formation efficiencies of globular clusters across cosmic time by modeling the formation and dynamical evolution of the globular cluster population of a Milky Way type galaxy in hierarchical cosmology, using the merger tree from the Via Lactea II simulation. All of the models are constrained to reproduce the observed specific frequency and initial mass function of globular clusters in isolated dwarfs. Globular cluster orbits are then computed in a time varying gravitational potential after they are either accreted from a satellite halo or formed *in situ*, within the Milky Way halo.

We find that the Galactocentric distances and metallicity distribution of globular clusters are very sensitive to the formation efficiencies of globular clusters as a function of redshift and halo mass. Our most accurate models reveal two distinct peaks in the globular cluster formation efficiency at $z \sim 2$ and $z \sim 7-12$ and prefer a formation efficiency that is mildly increasing with decreasing halo mass, the opposite of what expected for feedback-regulated star formation. This model accurately reproduces the positions, velocities, mass function, metallicity distribution, and age distribution of globular clusters in the Milky Way and predicts that $\sim 40\%$ formed *in situ*, within the Milky Way halo, while the other $\sim 60\%$ were accreted from about 20 satellite dwarf galaxies with $v_{cir} > 30$ km/s, and about 29% or all globular clusters formed at redshifts $z > 7$.

These results further strengthen the notion that globular cluster formation was an important mode of star formation in high-redshift galaxies and likely played a significant role in the reionization of the intergalactic medium.

Key words: (Galaxy:) globular clusters: general

1 INTRODUCTION

Globular Clusters (GCs), often referred to as fossils of ancient star formation, are compact gravitationally bound systems of $\sim 10^6$ stars which typically orbit a much larger host galaxy. These systems are among the oldest bound stellar objects known to exist, with some forming only a few hundred million years after the big bang. While these systems have been very well studied in the local Universe, their formation and evolutionary histories remain open questions in modern astrophysics.

Nearly all GCs are homogeneous in heavy elements (Sneden 2005), which suggests that the majority of their stars formed in an instantaneous burst with a high efficiency of gas-to-star conversion (James et al. 2004; Carretta et al. 2009). Despite the homogeneity of heavy elements within individual GCs, these systems are often classified into two categories: metal-poor with [Fe/H] $\leqslant -1.5$ and metal rich with [Fe/H] $\geqslant -1.5$. The origin of these two populations is unknown; however, this bimodality has been observed in multiple galactic environments (Zepf & Ashman 1993). Furthermore, the ages and kinematics of GCs also exhibit characteristic bimodal distributions.

Past observations have shown that galactic metal-poor

⋆ E-mail: hk380@ast.cam.ac.uk
† E-mail: ricotti@astro.umd.edu

GCs tend to be older than metal-rich GCs and the age spread in metal-poor GCs is ~ 1 Gyr compared to the ~ 6 Gyr dispersion in metal-rich GCs (Rosenberg et al. 1999; Salaris & Weiss 2002; Marín-Franch et al. 2009). There is some evidence of self enrichment in GCs; however, the age gap between metal-poor and metal-rich GCs is greater than the range present within each population suggesting that these are two distinct populations (Marín-Franch et al. 2009). However, more recent observations have shown a gradual trend of increasing age spread with increasing metallicity which weakens this age gap described in the previous works (Dotter et al. 2011; VandenBerg et al. 2013). Two different branches in the age versus metallicity plane have been identified which maintains the notion of two distinct populations.

Kinematically, multiple observations reveal that the red, metal-rich GCs are more spatially concentrated than the blue, metal-poor GC population (Pota et al. 2013; Schuberth et al. 2010; Faifer et al. 2011; Strader et al. 2011). Additionally, the metal-poor GCs tend to rotate less than the metal-rich GC population and the rotation of the metal-rich GCs has been associated with the photometric axis of the host galaxy (Pota et al. 2013). The distinct characteristics of these two populations suggests that they likely formed at different epochs and under different conditions.

Due to their old stellar populations, GCs today are faint and difficult to detect at large distances. However, Katz & Ricotti (2013) have shown that for $5-10$ Myrs after their formation, GC systems are very bright and can be detected in deep fields even at redshift $z = 8$. Although these systems are spatially unresolved, their UV luminosity functions and UV continuum slopes can be modeled and have characteristic signatures due to their bursting mode of star formation. It is therefore possible to set meaningful upper limits on their formation rate across multiple redshifts from $z = 8$ to $z = 1$. Katz & Ricotti (2013) concluded that GCs likely formed in two distinct epochs: $z > 6$ and $z < 3$. Additionally, Monte Carlo simulations convolving the age estimates of the Milky Way GCs with Gaussian ± 1 Gyr uncertainties, support the notion of a bimodal formation history. Katz & Ricotti (2013)'s results and the observed bimodal properties of these systems, suggest that there existed two distinct epochs of GC formation, with the old population possibly important for reionizing the intergalactic medium (Ricotti 2002). However, it is unclear if this scenario is consistent with the observed properties of Milky Way GCs and observations of GC systems in nearby isolated dwarfs. How did the Milky Way come to posses its current population of GCs? What fraction formed *in situ* within the Milky Way and what fraction was accreted onto the Milky Way via tidal disruption of merging dwarf galaxies? What role could GCs have played in the reionization of the Universe?

Many simulations have already been run attempting to address these questions. Prieto & Gnedin (2008) populated an N-Body simulation of a Milky Way type galaxy in order to determine if the ages, masses, metallicities and kinematics could be reproduced. The simulations were very successful in reproducing many of the observations however the model could not put good constraints on the when the GCs form and the mean distances of GCs were farther out than what is observed. Griffen et al. (2010) modeled both metal poor and metal rich GC formation in the Aquarius simulations by identifying both likely sites of GC formation in haloes with $T > 10^4$ K as well as a population that formed in the mergers of haloes. The formation epochs of GCs were constrained based on the role that the already formed GCs played in the reionization of the local medium.

We also aim to answer these questions by modeling GC formation in a high resolution N-body simulation of a Milky Way type galaxy and comparing characteristics of the resulting GC population with those properties exhibited by the Milky Way's GCs. Tuning the few free parameters in our simulations reveal new and unexpected insights into galaxy formation. We take a different approach than some of the previous simulations by matching the properties of the Milky Way GC population simultaneously to the characteristics of isolated dwarf GCs, which allows us to constrain the formation efficiencies of GCs across cosmic time and thus determine the role GCs may have played in the evolution of the Universe. This method is completely independent of the one used in Katz & Ricotti (2013), but interestingly seems to point to similar results.

All observational data for GCs was compiled using catalogs from the following references: Georgiev et al. (2009a,b); Forbes & Bridges (2010); Gnedin & Ostriker (1997); Strader et al. (2011); Galleti et al. (2004); Peacock et al. (2010); Harris (1996) (2010) Edition. In addition, this work made use of catalogs from Ochsenbein et al. (2000).

The paper is organized as follows: In Section 2, we describe the mechanisms responsible for the dynamical evolution of GCs. In Section 3, we propose a shape for the GC Initial Mass Function (GCIMF) as well as provide analytical calculations involving observations of GCs in local dwarfs to constrain the minimum formation efficiencies of GCs. We describe our simulations in Section 4 and interpret their results in Section 5. In Section 6, we present our discussion. In Section 7 we calculate the contribution of GCs to reionization and in Section 8, we discuss our conclusions.

2 MECHANISMS FOR THE DYNAMICAL EVOLUTION OF GLOBULAR CLUSTERS

The GC population that we observe today is likely a poor representation of the original GC population of a galaxy. Stellar evolution and dynamical effects, including two-body relaxation, dynamical friction, tidal shocks, and tidal truncation significantly reduce the number and mean mass of GCs from their epoch of formation to the present (Ostriker & Gnedin 1997; Fall & Zhang 2001). Our treatment of the dynamical evolution of GCs follows closely the one in Prieto & Gnedin (2008), with a few differences that will be emphasized as we describe the details of the model.

We assume that all dynamical effects are independent of each other and the GC's mass, M_{gc}, is governed by the following differential equation:

$$\frac{dM_{gc}}{dt} = -(\nu_{se}(t) + \nu_{ev}(t) + \nu_{sh}(t))M_{gc}, \qquad (1)$$

where ν_{se}, ν_{ev}, ν_{sh} are the respective mass-loss rates due to stellar evolution, two-body relaxation, and tidal shocks (Fall & Zhang 2001; Prieto & Gnedin 2008). While the assumption that these processes are independent is simplistic, it is certainly well motivated due to the distinct time scales over which each mechanism operates.

We adopt a Kroupa stellar IMF for the GCs (Kroupa 2001) which has a mean mass of $\bar{m} \approx 0.387$ M$_\odot$ after the high mass stars ($M > 2$ M$_\odot$) have died off. Within the first 300 Myr, about 30% of the initial mass of the GC is lost due to stellar evolution. This time scale is very short compared to the typical ages of GCs. For a detailed description and calculation of stellar evolution, we refer to section 3.1 of Prieto & Gnedin (2008).

For two-body relaxation, we refer to the approximation derived by Spitzer (1987),

$$\nu_{ev} = \frac{7.25 \xi_e \bar{m} G^{1/2} \ln \Lambda_{cl}}{M_{gc}^{1/2} R_h^{3/2}}, \quad (2)$$

where $\xi_e = 0.045$ is a normalization factor derived by Hénon (1961). The parameter $\ln \Lambda_{cl}$ is the time-dependent coulomb logarithm which is derived by Binney & Tremaine (1987) to be between 10 and 12 and we have chosen $\ln \Lambda_{cl} = 12$. As described later, our simulated GCs are modeled with constant density as they evolve, which causes the mass loss due to two-body relaxation alone to be constant as a function of time for all GCs (i.e. $\nu_{ev} \propto M_{gc}^{-1}$). Furthermore, this process is ineffective at destroying GCs during the first few hundred Myrs in the GC life cycle and only becomes important at later times. Because the time scales over which stellar evolution and two-body relaxation operate are clearly distinct, we treat them independently.

For disk shocking we refer to the approximation in Prieto & Gnedin (2008) with a slight modification:

$$\nu_{sh} = \begin{cases} \frac{5/3}{\Delta t} \frac{I_{tid} R_h^3}{G M_{gc}} & \text{if } sign(z(n-1)) \neq sign(z(n)), \\ 0 & \text{if } sign(z(n-1)) = sign(z(n)), \end{cases} \quad (3)$$

where n is the current time step corresponding to a time t and $n-1$ is the time corresponding to the previous time step. This ensures that disk shocking is only effective when the sign of the z-coordinate changes between time steps indicating that the GC has crossed the plane of the disk. Δt is the length of the time step in our integration routine for the GCs orbits and $I_{tid} \sim 4 g_m^2 / V_z^2$. The parameter g_m is the maximum vertical acceleration and V_z is the component of the GC's velocity orthogonal to the disk. It is clear that this is an instantaneous process and can therefore be treated separately from both stellar evolution and two-body relaxation.

When the half mass radius, R_h, of a GC approaches its tidal radius, R_t, large percentages of stars can be stripped, significantly decreasing its mass. The tidal radius of the GC then shrinks due to this loss in mass, allowing more stars to escape. This process is unstable, resulting in the destruction of the GC on a relatively short timescale (Baumgardt 1998). Baumgardt (1998) define a critical value x_{crit} such that if the ratio $R_h / R_t \geqslant x_{crit}$ then the GC is destroyed. We choose $x_{crit} = 0.37$, which is more conservative than what was chosen in Baumgardt (1998). This was tuned to correspond to less than a few hundred pc from the galactic center in our model and we believe this assumption is well motivated given that no GCs are observed within a few hundred parsecs of the galactic center. Furthermore, we emphasize that regardless of the choice of x_{crit}, since we will model the GCs as having constant density, this process effects all GCs in our model equally. As we will later discuss, this mechanism only controls the overall normalization of GCs in our model which is a parameter that we can only bound with upper and lower limits rather than make an explicit prediction. We define R_t, consistent with Baumgardt (1998) as:

$$R_t \equiv \left(\frac{M_{gc}}{3 M_{gal}(< R_{gc})} \right)^{1/3} R_{gc}, \quad (4)$$

where R_{gc} is the distance of the GC from the galaxy and M_{gal} is the mass of the galaxy inside R_{gc}.

Finally, we also compute the acceleration due to dynamical friction using the Chandrasekhar formula (Chandrasekhar 1943) as given by Binney & Tremaine (1987) assuming that the $M_{gc} >> m$, where m is the mass of the dark matter particles (when the gravitation potential is dominated by the dark matter halo) or bulge stars:

$$\frac{d\vec{v}_{gc}}{dt} = -\frac{4\pi G^2 \rho M_{gc} \ln \Lambda}{v_{gc}^3} \left[erf(X) - \frac{2X}{\sqrt{\pi}} e^{-X^2} \right] \vec{v}_{gc}, \quad (5)$$

where here we define $\Lambda \equiv b_{max} V_C^2 / (G M_{gc})$ with b_{max} being the impact parameter, and V_C is the speed of the GC through the galaxy which we calculate by integrating the orbit, but can also be roughly estimated as the local circular velocity. Here, ρ is the local density of the galaxy, $X \equiv v_{gc} / (\sqrt{2}\sigma)$ and σ is the velocity dispersion of the dark matter particles (or bulge stars).

For an approximate test of the validity of these approximations, we can take an analytical approach to modeling the destruction of 140 Milky Way GCs using their measured masses and half light radii. Plotted in Figure 1 is the "vital diagram", first created by Ostriker & Gnedin (1997) for both the Milky Way and M31. Since almost all GCs reside within the triangle defined by lines of constant dynamical friction timescale (upper horizontal line), two-body relaxation timescale (left side of the triangle), and tidal destruction timescale (right side of the triangle), we can be confident that our approximations are fairly accurate.

2.1 Dynamical Evolution in Dwarf Galaxies

While these approximations are accurate for the Milky Way and M31 GC populations, one might ask whether the same can be said for GCs in dwarf galaxies. The naive expectation is that dynamical friction should be enhanced while tidal destruction is minimized. It is interesting to note that the GCs in dwarf galaxies tend to occupy roughly the same locations in $M - R_h$ space as the GCs in the Milky Way and M31, as shown in the right panel of Figure 1. It seems there is a slight tendency for GCs in the local dwarfs to occupy some of the lower density space compared to GCs in M31 and the Milky Way, pointing to a less efficient tidal destruction rate due to the lower density of dwarf galaxies. Furthermore, we note that the mass function of GCs in dwarf galaxies shows a higher abundance of GCs at lower mass compared to the Milky Way, as illustrated in Figure 2. It is these GCs which are more susceptible to destruction from tides and this higher abundance may also point to tides being inefficient in dwarf galaxies.

The Fornax dwarf spheroidal galaxy is the Milky Way's largest dwarf spheroidal and it has a system of five GCs ranging in mass from 3.7×10^4 $M_\odot - 3.63 \times 10^5$ $M_\odot$ at distances of $0.24 - 1.6$ kpc (Angus & Diaferio 2009). Multiple studies

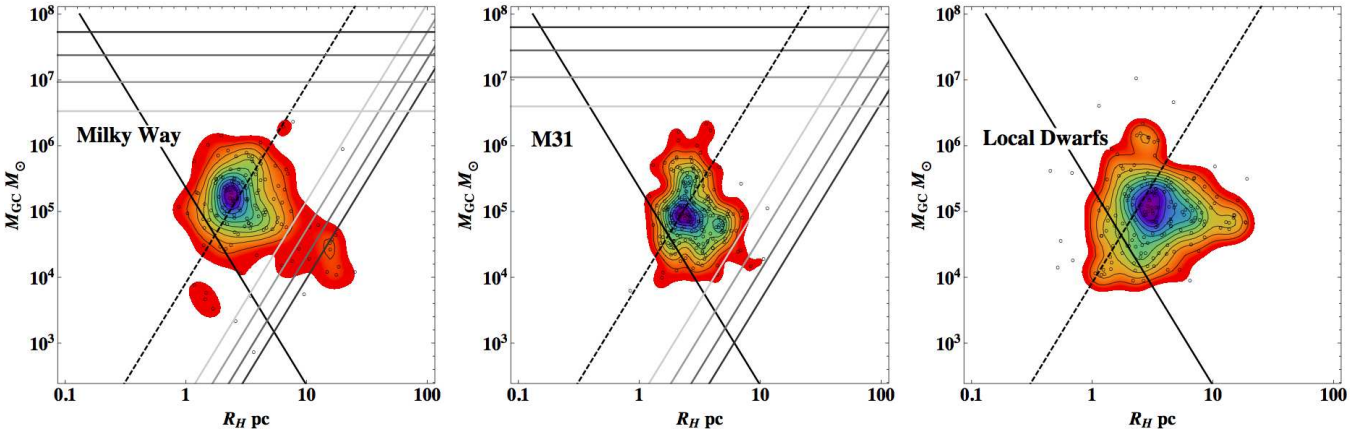

Figure 1. *Left.* Vital diagram for Milky Way GCs. *Center.* Vital diagram for M31. *Right.* Vital diagram for GCs in local dwarf galaxies. For the data we show both the data point and the normalized density distribution function. The left side of the triangle is the theoretical line for relaxation. The right side lines are the theoretical lines for tidal destruction and the top lines are theoretical lines for dynamical friction. Different lines for tidal destruction and dynamical friction represent different initial positions for the GCs corresponding to 12, 7, 5, 3 kpc respectively. All of these lines were computed with the assumption that the GCs are 12 Gyr old. The majority of Milky Way's and M31's GCs fit in this triangle which verifies our assumptions are valid. We do not plot the top and right sides of the triangle for the GCs in local dwarfs because these lines are unique for each galaxy whereas our sample is from multiple different dwarfs. The dotted black line in the left and center panels represent the constant density we use to model GCs in our simulations. Data for the Milky GCs is from Georgiev et al. (2009a), data for M31 is from Strader et al. (2011) and data for GCs in local dwarf galaxies is from Georgiev et al. (2009b). The mass model we use for the Milky way is from Irrgang et al. (2013).

(Goerdt et al. 2006; Read et al. 2006; Sánchez-Salcedo et al. 2006; Inoue 2009) have claimed that these GCs should have fallen to the center of the host galaxy in much less than a Hubble time due to dynamical friction. The Fornax dwarf spheroidal does not show evidence of a bright nucleus where the sinked GCs would reside (Angus & Diaferio 2009). We found similar contradictory results on the effect of dynamical friction in dwarfs looking at a large sample of dwarf galaxies from Georgiev et al. (2010).

Multiple groups, such as the ones listed previously have attempted to resolve this issue but there has not been an agreed upon conclusion. While this outcome clearly demonstrates a lack of understanding of the system, it provides an interesting prospect: if dynamical friction is ineffective, GCs survive in their host galaxy longer than expected and are more easily accreted onto a larger galaxy if the dwarf galaxy falls into a deeper gravitational well. In addition, if GCs reside closer to the tidal radius of the dwarf galaxy, then as soon as the dwarf approaches a much larger galaxy, the GCs will be accreted nearly instantly. Although we do not understand why the GCs are not sinking in the Fornax dwarf spheroidal and other local dwarfs, this seems a common pattern among GCs in dwarf galaxies. Hence, a large fraction of old metal-poor GCs in the Milky Way have likely been accreted from dwarf satellites rather than formed *in situ*.

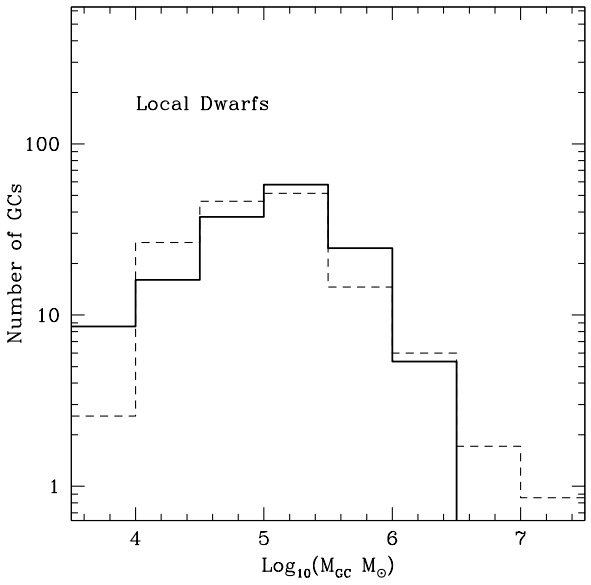

Figure 2. Mass function of GCs in local dwarf galaxies from Georgiev et al. (2010) (dashed line) compared to that of the Milky Way (thick line). The histogram has been normalized to a population of 150 GCs. The excess of low mass GCs may suggest that tidal effects are inefficient in disrupting GCs in dwarf galaxies.

3 CONSTRAIN THE GC'S MASS FUNCTION AND FORMATION EFFICIENCIES FROM DWARF GALAXIES

3.1 The GC's Mass Function in Dwarf Galaxies

The exact shape and normalization of the GCIMF remains reasonably unconstrained; however, multiple groups have shown that a power law or Gaussian GCIMF can lead to the right shape for the GCs in the Milky Way when the dynamical evolution is simulated (Fall & Zhang 2001; Prieto & Gnedin 2008). Dwarf galaxies offer an ideal environment to determine the initial mass function and formation efficiency of GCs. Some dynamical processes that are important in more massive galaxies, like the Milky Way, can

be neglected, therefore rendering the calculations more robust. Since the effects of tidal shocking and tidal truncation are minimized for high density GCs in isolated dwarf galaxies, the high mass end of the GC mass function in dwarf galaxies should be representative of the GCIMF.

Modeling the evolution of the GC mass function in dwarf galaxies is thus quite simple. Stellar evolution destroys $\sim 30\%$ of a GC mass within the first few Myr of its lifetime, and using our assumption that each GC maintains its initial density during its evolution, two-body relaxation is easily modeled as a constant mass loss proportional to the age of the GC. If we suppose that the shape of the GCIMF is a power law with slope α, the subsequent evolution transforms the mass function to the form:

$$\frac{dN}{dM} \propto (M + M_{2bd})^{\alpha}, \tag{6}$$

where $M_{2bd} \propto t$ is the mass loss due to two-body relaxation. For $M \gg M_{2bd}$, this equation reduces to $dN/dM \propto M^{\alpha}$ and for $M \ll M_{2bd}$, we get $dN/dM \propto M_{2bd}^{\alpha} = const.$

Letting the slope of the GCIMF and the mass loss due to two-body relaxation be free parameters, we can constrain the density of GCs as well as the slope of the GCIMF by fitting the mass function of GCs in local dwarf galaxies. In the left panel of Figure 3, we show the one and two sigma confidence limits for M_{2bd} and α. The best fit values are $\alpha = -2.05$ and $M_{2bd} = 1.1 \times 10^5\ M_{\odot}$. Assuming and average age of GCs of 12 Gyrs, using equation (2) we derive an average GC density of 2000 $M_{\odot}/pc^3$, which is consistent with the average density of GCs in both the Milky Way and M31 (see Figure 1). In the right panel of Figure 3 we show the best fit model for the GC's mass function compared data from local dwarf galaxies.

In Appendix A we relax the assumption that all GCs have constant mean density. We keep the assumption that GCs maintain a constant density as they evolve, but we explore the case in which the initial density of each GC is related to their mass. To test this idea, we assume that all GCs have a constant R_h so that $\rho_h \propto M_{gc}$. However, using this model we are unable to match simultaneously the shape of the mass function in dwarfs and the Milky Way GCs. For this reason we only consider the constant density model in the rest of this paper.

3.2 Constraints on GC's Formation Efficiencies

While the shape of the GCIMF dictates the relative efficiency of low mass and high mass GC formation, the overall normalization remains unconstrained. The bottom panel of Figure 4 in Georgiev et al. (2010) shows that late type and early type dwarf galaxies in their sample with absolute visual magnitude brighter than -16.5 contain at least one observed GC. This data, in combination with the mass loss rates and destruction rates of GCs, estimated in the previous section, can be used to constrain the GC formation efficiency as a function of redshift for both red and blue dwarf galaxies.

Stellar evolution alone removes about 30% of the initial mass of all GCs within the first hundred few Myr, assuming a Kroupa stellar IMF. Thus, given an initial total mass in GCs, M_{gc}^{ini}, the effect of stellar evolution is to keep the number of GCs constant but reduce the total mass in GCs and each individual GC mass by a factor of 0.7. Assuming a GCIMF with a power-law slope of $\alpha = 2$ as derived in § 3.1, the mean GC mass is $\langle m_{gc} \rangle^{ini} = M_{low} \ln(M_{up}/M_{low})$, and thus, the initial number of GCs is $N^{ini} = M_{gc}^{ini}/\langle m_{gc} \rangle^{ini}$. For our fiducial model with $M_{low} = 10^5$ $M_{\odot}$ and $M_{up} = 2.857 \times 10^7$ $M_{\odot}$, we have $\langle m_{gc} \rangle^{ini} = 5.2 \times 10^5$ $M_{\odot}$.

The number of GCs that survive two-body relaxation and mass loss due to stellar evolution can be estimated analytically from dN/dM given in equation (6):

$$\begin{aligned} N^{surv} &= \int_{M_{low}^*}^{M_{up}} \frac{dN}{dM} dM \\ &= N^{ini} \frac{M_{low}}{M_{low}^*} = N^{ini} Min[1, 0.7 M_{low}/M_{2bd}], \end{aligned} \tag{7}$$

where we define $M_{low}^* = Max[M_{low}, M_{2bd}/0.7]$. We define the number of surviving GCs, $N^{surv} \equiv f_N^{surv} N^{ini}$, for our fiducial model and $M_{2bd} = 1.1 \times 10^5 (t/12\ Gyr)$ $M_{\odot}$ derived in Section 3.1 and we, therefore, find

$$f_N^{surv}(t) = Min\left[1, 63.6\% \left(\frac{M_{low}}{10^5 M_{\odot}}\right)\left(\frac{12\ Gyr}{t}\right)\right]. \tag{8}$$

Similarly, the surviving fraction by mass is

$$\begin{aligned} f_M^{surv}(t) &= \frac{\langle m_{gc} \rangle^{2bd}}{\langle m_{gc} \rangle^{ini}} f_N^{surv} \\ &\approx \frac{56\%}{1 + \ln(10^5\ M_{\odot}/M_{low})/5.65} \text{ at t=12 Gyr}, \end{aligned} \tag{9}$$

where

$$\begin{aligned} \langle m_{gc} \rangle^{2bd} &= 0.7 M_{low}^* \ln\left[\frac{M_{up}}{0.7 M_{low}^*}\right] - M_{2bd} \\ &= \begin{cases} 0.7 \langle m_{gc} \rangle^{ini} - M_{2bd} & \text{for } M_{2bd} < 0.7 M_{low}, \\ M_{2bd}\left(\ln\left[\frac{M_{up}}{M_{2bd}}\right] - 1\right) & \text{for } M_{2bd} > 0.7 M_{low}. \end{cases} \end{aligned} \tag{10}$$

For the fiducial values adopted here $\langle m_{gc} \rangle^{2bd} = 5 \times 10^5$ $M_{\odot}$ at $t = 12$ Gyr. Our calculation assumes that tidal effects in dwarf galaxies can be neglected and the mass loss due to stellar evolution and two-body relaxation alone represents the majority of the mass loss. Assuming, as explained later, that the total mass in GCs at formation[1] is

$$M_{gc}^{ini} \equiv \eta_i 7 \times 10^9\ M_{\odot} \left(\frac{M_{dm}}{7 \times 10^9\ M_{\odot}}\right)^{1+\gamma}, \tag{11}$$

and adopting the analogous definition for the formation efficiency η after evolutionary effects we have

$$\eta = \eta_i f_M^{surv}. \tag{12}$$

Finally, adopting a mass-to-light relationship for dwarfs, $L_V \approx 2.6 \times 10^8\ L_{\odot} (M_{dm}/7 \times 10^9\ M_{\odot})^{5/3}$, as in Georgiev et al. (2010), we obtain for the fiducial model:

$$N_{gc}^{surv}(t) = f_N^{surv} \eta_i \left(\frac{7 \times 10^9}{\langle m_{gc} \rangle^{ini}}\right)\left(\frac{L_V}{2.6 \times 10^7\ L_{\odot}}\right)^{\frac{3(1+\gamma)}{5}}. \tag{13}$$

From Figure 4 in Georgiev et al. (2010), it is clear that red dwarf galaxies have a larger N_{gc}^{surv} than the blue ones at fixed luminosity, for $M_V \leqslant -12$. Within the working assumption that the adopted mass-to-light ratio of the dwarfs

[1] We have normalized this equation to a mass of 7×10^9 $M_{\odot}$ because this is the normalization we use in our simulations which corresponds to a V_C of 50 km/s.

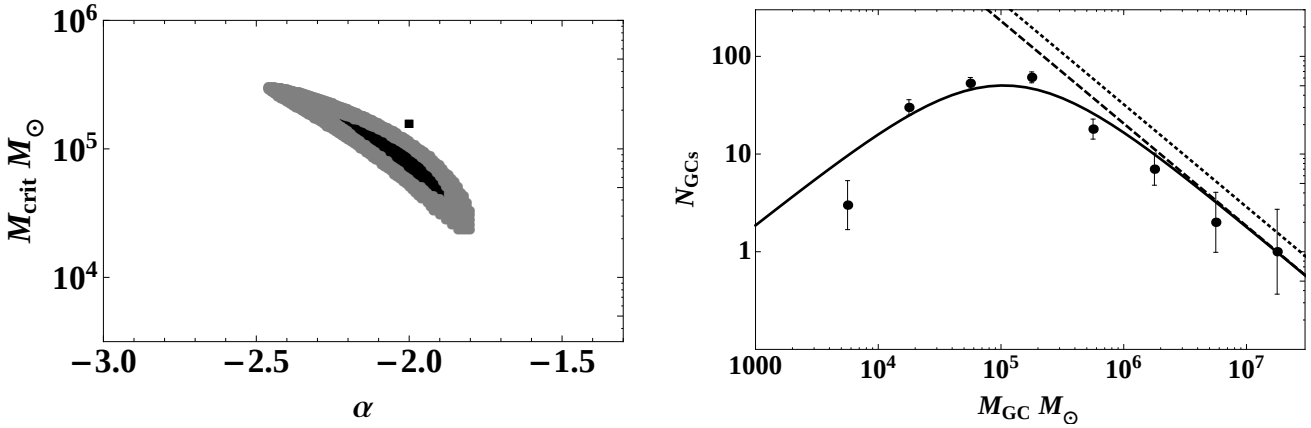

Figure 3. *Left.* Parameter space analysis of the best fit slope and critical mass for the GCIMF for the constant density model. The black and gray regions are the 1σ and 2σ confidence levels respectively. The square represents the parameters used in Prieto & Gnedin (2008). *Right.* Our chosen GCIMF parameters compared with the dwarf galaxy GCMF for the constant density model.

is the same for blue and red galaxies, this result points to a larger η_i for early type dwarf galaxies (also consistent with assuming a larger η_i at high redshift). Additionally, the number of surviving GCs remains relatively constant with decreasing luminosity for early type dwarfs, pointing to a small value of $1+\gamma$, or $-1<\gamma<0$.

Inspecting Figure 4 in Georgiev et al. (2010) we see that all (red and blue) dwarf galaxies with luminosity $L\sim 5.4\times10^8$ $L_\odot$ have at least one GC. At this luminosity we set $N_{gc}^{surv}=1$ to derive a rough estimate of the minimum formation efficiency to produce at least one surviving GC. The slope of the curve at $M_V\leqslant -12$ for the fraction of dwarfs with at least one observed GC as a function of luminosity gives $\gamma\sim-0.8$. There are only a few galaxies in the magnitude bins dimmer than $M_V=-12$ and thus we only fit this curve for brighter magnitude bins. From Equation (13) we derive the efficiency of GC formation in early type dwarfs to be

$$\eta_i(t)^{red}\approx 6.8\times10^{-5} f_N^{surv}(t)^{-1}. \quad (14)$$

Similarly, for late type dwarfs we obtain $\gamma\sim-0.35$ and

$$\eta_i(t)^{blue}\approx 5.5\times10^{-5} f_N^{surv}(t)^{-1}. \quad (15)$$

In conclusion, these two values of η_i and γ bracket the mean formation efficiency of GCs in dwarf galaxies as a function of time. These results also point to a *GC formation efficiency either constant or increasing with decreasing galaxy mass*, the opposite of what expected due to feedback effects for "normal" star formation in dwarf galaxies. In addition, the large scatter (of nearly two orders of magnitude) of the specific frequency at a fixed galaxy luminosity may be accommodated in models in which η_i varies as a function of cosmic time by a similar amount. In Figure 5, we plot how minimum values of η_i vary with time.

Note that in Georgiev et al. (2010) and other studies, the GC formation efficiency, η, is defined as $M_{gc}^{surv}\equiv\eta M_{dm}$, analogously to our definition of η given by Equation (12) assuming $\gamma=0$. Georgiev et al. (2010) have found that $\eta\approx5\times10^{-5}$ which is consistent with Blakeslee (1999), who found $\eta\approx1.71\times10^{-4}$, and other studies including, Kravtsov & Gnedin (2005) and Spitler & Forbes (2009). This value is the observed efficiency which is post stellar evolution and dynamical processes. The initial GC formation efficiency prior to stellar evolution and dynamical processes, η_i, is a free parameter in our simulations. For whatever η_i we choose, we are constrained by observations of dwarf galaxies to a range of values $10^{-5}<\eta<10^{-4}$.

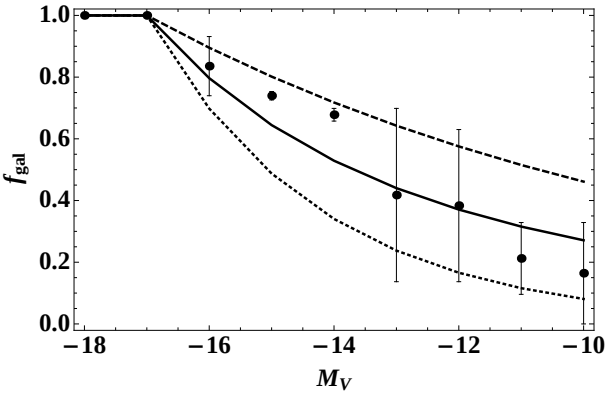

Figure 4. The percentage of galaxies expected to host at least one GC as a function of the absolute visual magnitude of the host galaxy for 12 Gyr old GCs. The dashed line represents the expectations for red galaxies and the dotted line represents the expectations for blue galaxies. The black line is the mean of the two types of galaxies. The data points are the average of the blue and red galaxies that host at least one GC from Georgiev et al. (2010). Error bars on data points correspond to the range between red and blue galaxies and the true dispersion in the mean of all galaxies is likely larger than what is plotted.

4 MODELING GC FORMATION, ACCRETION, AND DYNAMICAL EVOLUTION

4.1 The Via Lactea II Simulation

We use the halo merger tree from a high resolution N-body simulation, the Via Lactea II (VL II) (Diemand et al. 2008),

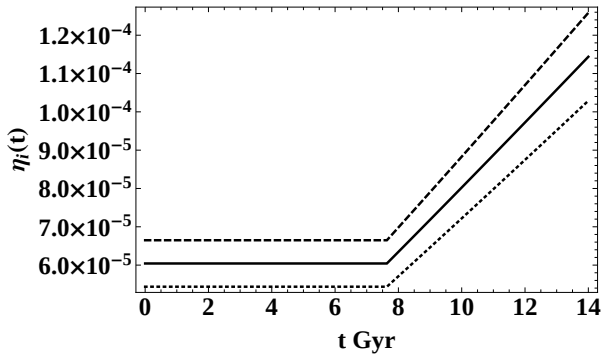

Figure 5. We show the minimum formation efficiencies, $\eta_i(t)$, as a function of time for our best fit GCIMF for the UDM. The dashed line is for red galaxies, the dotted line is for blue galaxies, and the black line is the mean of the two types of galaxies.

to model the formation, accretion, and dynamical evolution of GCs in a Milky Way type halo and in a few isolated dwarfs around the main halo. The VL II simulation is a cosmological N-body simulation of over 1 billion particles with mass resolution of 4.1×10^3 M$_\odot$. The simulation starts at $z = 104.3$ in a 40 comoving Mpc periodic box using cosmological parameters from WMAP 3 (Spergel et al. 2007). At $z = 0$, the main halo is representative of a Milky Way type galaxy with $r_{200} = 402.1$ kpc, $M_{200} = 1.917 \times 10^{12}$ M$_\odot$ and a maximum circular velocity of $V_{cir,max} = 201.3$ km/s (note that here the subscripts refer to mean halo density 200 times the cosmic value, not 200 times the critical density). We utilize the publicly available evolutionary tracks of the 20,000 largest haloes and subhaloes at $z = 4.56$ as well as the complete merger tree (Diemand private communication). The time evolution is sampled uniformly after $z = 7.77$, but rather coarsely ($\Delta t = 687$ Myr) with 27 outputs from the simulation beginning at $z = 27.54$ to the end at $z = 0$.

4.2 Distributing GCs to Haloes

As described in Section 3.2 and in Equation (11), we choose to parameterize the number (and total mass) of GCs in a halo, at any given time, as a fraction of the dark matter mass of the host. The number of GCs we attribute to each halo at the time of virialization (which we define to be when a halo reaches its maximum V_{max}) is:

$$N_{GC} = \tilde{\eta}_i(z, M_h) \frac{M_h}{\langle m_{gc} \rangle^{ini}}, \tag{16}$$

with specific GC formation efficiency

$$\tilde{\eta}_i(z, M_h) \equiv \eta_i(z) \left(\frac{M_h}{7 \times 10^9 \ M_\odot} \right)^\gamma, \tag{17}$$

where $\eta_i(z)$ is a function of redshift, and γ is a free parameter describing the dependence of the GCs formation efficiency on the halo mass. We choose a pivot point for the dependence of η_i on halo mass appropriate for dwarf galaxies. Because the masses of haloes in the simulation are environmentally dependent (and somewhat arbitrarily defined in N-body simulations), we choose to relate N_{GC} to the maximum circular velocity of the halo, V_{max}, rather than the halo mass. This assumption is also convenient to define a redshift of formation of a halo and whether a subhalo is being tidally stripped. Indeed V_{max} reaches its maximum value at the redshift of virialization and remains roughly constant afterwards, unless the halo is being tidally stripped. Hence, we define M_h consistent with the parameters for the Milky Way as follows:

$$M_h = 1.25 \times 10^{12} \ M_\odot \left(\frac{V_{max}}{220 \ km/s} \right)^{\beta'}, \tag{18}$$

where β' in general depends on the halo mass (and redshift of formation) and has a value between 3 and 4. We adopt a fiducial value $\beta' = 3.5$ that gives $M_h = 7 \times 10^9 \ M_\odot (V_{max}/50 \ km/s)^{3.5}$, also appropriate for dwarf galaxies. Combining Equations (16)-(18), we define our model for *in situ* formation of GCs:

$$N_{GC} = \eta_i(z) \frac{7 \times 10^9 \ M_\odot}{\langle m_{gc} \rangle^{ini}} \left(\frac{V_{cir,max}}{50 \ km/s} \right)^{\beta}, \tag{19}$$

where we allow for $\beta \equiv \beta'(1 + \gamma) \neq \beta'$, if the GC formation efficiency depends on the halo mass in addition to the redshift of virialization of the host halo. Values $\beta < \beta'$ indicate that dwarf galaxies have a higher *in situ* GC formation efficiency per unit halo mass than Milky Way sized galaxies. We will explore this model in Section 5.3.

Equation (19) also determines the minimum circular velocity of a halo that forms at least one GC. Because η_i varies with redshift, the minimum circular velocity defined by this equation is a function of z and β. We have chosen $\beta = 3.5$ (*i.e.*, $\gamma = 0$) for our fiducial model. However, as discussed in Section 3.2, data on local dwarf galaxies by Georgiev et al. (2010) show that early type and late type dwarfs have different values of γ and η_i, hence suggesting that these parameters depend on redshift.

We assign GCs to the haloes when they have reached their maximum V_{max}, which indicates that they have just virialized. Other groups, including Prieto & Gnedin (2008) define a truncation redshift, z_t, after which GCs can no longer form. This is certainly a major assumption of our model as the formation mechanisms of GCs have yet to be resolved (excluding the GCs we see forming in mergers which are discussed later). The formation epochs we define for GCs should have little effect on the kinematics of the final surviving population because we will demonstrate that all GCs in our models are equally susceptible to tidal effects. As long as the GCs are formed prior to dwarf being accreted onto the main halo, our results will be robust to this parameter. Small variations in the formation epochs will only have marginal effects on the mass function because two body relaxation is the only mechanism for which the time dependence is explicit, prior to the time of accretion onto the main halo. We refrain from advocating for one of the many proposed mechanisms for the formation of GCs as this is not the focus of the current work. We emphasize that as long as the GCs have formed in the dwarf haloes prior to the accretion epoch, our model is very robust.

We assign a mass to each GC by randomly drawing from the chosen GCIMF. We adopt a constant density model for the internal structure of each GC. While this model may seem too simplistic, Prieto & Gnedin (2008) found that their model using GCs with a constant half-mass density of $\rho_{GC} = 4 \times 10^3$ M$_\odot$pc^{-3} best reproduced the mass function of the Milky Way metal poor GCs. In Section 3.1 we found sim-

ilar results testing a constant and a variable initial density model. Here we also adopt the constant density model however with a slightly different density $\rho_{GC} \approx 2 \times 10^3$ M$_\odot$pc^{-3} constrained to reproduce the mass function of GCs in local isolated dwarfs (see Section 3.1).

4.3 Accretion and Dynamical Evolution

We divide the GCs in our simulation into three distinct categories: 1) GCs which form in a specific halo that survive to the present without merging with a larger halo (*i.e.*, *in situ* formation of GCs in dwarf galaxies or in the main halo). 2) GCs formed in haloes which are accreted by another halo and remain outside the virial radius of the Milky Way halo (*i.e.*, GCs accreted by dwarf galaxies). 3) GCs which are eventually accreted by the Milky Way halo.

(i) For the first class of GCs, we compute stellar evolution and two-body relaxation beginning at the epoch of formation. A GC is considered destroyed when its mass becomes less than 10^4 M$_\odot$. This mass threshold is chosen by looking at the catalog of GCs in nearby dwarf galaxies (Georgiev et al. 2010). There are very few GCs with mass less than 10^4 M$_\odot$, which is likely a result of the rate of destruction being fast at these masses and partially an observational bias. We do not compute the GCs' orbits in this case because GCs are weakly affected by tidal destruction in low surface brightness dwarf galaxies. The densities of the GCs are larger than the stellar and dark matter densities in dwarfs and justifying why minimal tidal destruction is to be expected for this specific population of GCs. Thus stellar evolution and two-body relaxation are the main modes of GC destruction in dwarfs, allowing us to analytically reproduce the mass function of GCs in nearby dwarf galaxies.

The one exception to this assumption holds for the GCs that form *in situ* in the Milky Way's progenitor halo, or along with the main halo in the simulation. For these GCs, we compute the orbits as well as dynamical friction, tidal shocks, and tidal destruction along with two-body relaxation and stellar evolution as described in Section 2.1. For the GCs that form *in situ* in the Milky Way, we distribute them randomly in a uniform density sphere within 1.5 disk scale lengths and with velocities smaller than the local V_C so that they are dynamically cold. We have tested the effect of changing the volume of the sphere and the magnitude of the initial velocity and note that there is not much difference except when the GCs are placed well within the bulge or much farther than the disk size. We find our simulations to be largely insensitive to these parameters.

(ii) The second class of GCs is very similar to the first, but includes GCs accreted onto dwarf galaxies from satellites, in addition to *in situ* formation. For the same reasons previously stated, we do not compute orbits and evolve the GC mass function with only stellar evolution and two-body relaxation. We define the accretion epoch to be the redshift at which V_{max} of the satellite halo becomes smaller than a fraction $f = 70\%$ of the maximum V_{max}^{max} over all redshifts. At this time, tidal interactions are affecting the inner part of the halo and we assume that GCs are stripped from their host and accreted. In order to determine the halo onto which the stripped GCs are accreted, we use the full merger tree of the simulation. We search for the closest halo with a mass greater than our tidally disrupted halo and define this as the new host. GCs can undergo multiple accretion events throughout cosmic time.

(iii) The third class of GCs is perhaps the most interesting, as these are GCs that are eventually accreted onto the Milky Way halo. Prior to accretion, we compute stellar evolution and two-body relaxation as in the previous two categories. However, if a halo's V_{max} drops to below $f = 70\%$ of its maximum V_{max}^{max} and this halo is within the virial radius of the Milky Way halo, the GCs are accreted onto the Milky Way halo and we begin computing their orbits including the effect of dynamical friction, tidal destruction, and tidal shocks. We use the velocity of the disrupted host as the initial velocity for all accreted GCs associated with this halo. Additionally, we offset the position of each GC in the satellite halo by randomly assigning their position within spherical shells. We limit the radial coordinates of each GC to be within the tidal radius at the time output before accretion and the tidal radius at the epoch of accretion. It is important to note that our simulations results are rather insensitive to our choice of f. This is likely because the orbits of accreted GCs depend mainly on the velocity of the GCs host at the time of the accretion rather than its exact position along the orbit. The position of the GCs when accreted are not well resolved due to the coarse time resolution of our merger tree, that consists of only 27 redshift outputs, that we use to interpolate the orbits of galaxies and satellites. This coarse time step is unlikely to fully resolve the infall of the satellite due to dynamical friction, possibly leading to a slight error on the position and time in which we define the destruction epoch for each dwarf halo.

We note that our definition of accretion epoch is slightly different than some other uses in the literature. Prieto & Gnedin (2008) begin orbits of GCs at the point when the dwarf enters within the virial radius of the main halo. Griffen et al. (2010) consider the GCs as part of the main halo their simulations when the GC are within twice the half mass radius of the main halo at z=0. The epoch of accretion of the dwarf would certainly be when the dwarf becomes gravitationally bound to the main halo; however, the important definition for this work is the epoch at which the globular clusters are stripped from the dwarf haloes (which is what we have defined as the accretion epoch). This is more likely to be at the time when the dwarf begins to be tidally disrupted as we have described.

We use a time evolving model for the simulated Milky Way galaxy that includes a dark matter halo, a disk, and a bulge. The evolution of the dark matter halo is taken directly from the 27 outputs of the VL II simulation. We use cubic splines to interpolate between the simulation outputs. We use a Miyamoto-Nagai potential (Miyamoto & Nagai 1975) to describe the disk and a Plummer sphere to describe the bulge (Plummer 1911):

$$\Phi_{halo}(r) = -\frac{GM_*}{r_s}\frac{ln(1+(r/r_s))}{r/r_s}, \qquad (20)$$

where $M_* = 4\pi\rho_s r_s^3$ and $\rho_s = 4\rho(r_s)$,

$$\Phi_{disk}(R,z) = -\frac{GM_{disk}}{\sqrt{R^2 + (a_d + \sqrt{z^2 + b_d^2})^2}}, \qquad (21)$$

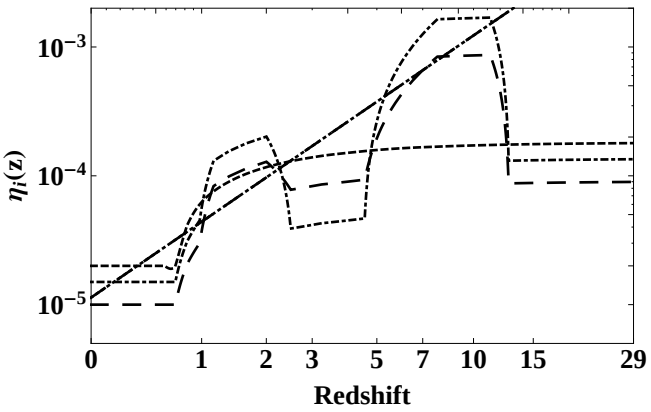

Figure 6. Formation efficiencies for the CE (short dashed), KR13 (long dashed), KR13-bis (short dot dashed), and Power Law (long dot dashed) models.

$$\Phi_{bulge}(r) = -\frac{GM_{bulge}}{\sqrt{r^2 + b_b^2}}. \quad (22)$$

We adopt a scaling relation between the mass of the disk to be 4.5% of the mass of the halo at all redshifts, slightly less than Klypin et al. (2002); Prieto & Gnedin (2008), and supported by observations. Thus, the mass of the disk at a given redshift is $M_d(z) = (0.045 M_h(z))$. We choose $a_d(z) = 0.01 r_{200}(z)$ and $b_d(z) = 0.054 a_d(z)$, consistent with the values for the Milky Way (Paczynski 1990) and a smaller bulge than (Paczynski 1990) which is also scaled with time. We note that it is more likely that the Milky Way has a bar rather than a classical bulge and since we use a classical bulge, we satisfy the constraint that the mass of the bulge is not greater than $\sim 8\%$ of the mass of the disk and use an extended bulge (Shen et al. 2010). Because the mass of the bulge is low compared to the rest of the galaxy, only orbits that approach the center are likely effected; however, these GCs are also more prone to destruction given the higher density of the bulge compared to the rest of the galaxy. In summary, the $z = 0$ Milky Way parameters we adopt are: $M_{200} = 1.94 \times 10^{12}$ M$_\odot$, $r_{200} = 462.274$ kpc, $M_{disk} = 8.60 \times 10^{10}$ M$_\odot$, $a_d = 4.623$ kpc, $b_d = 0.25$ kpc, $M_{bulge} = 5 \times 10^9$ M$_\odot$ and $b_b = 0.540$ kpc.

We use a leap frog integrating scheme with a constant time step of 1 Myr (determined by convergence tests) to follow the orbits of the GCs around the time evolving potential. We compute stellar evolution, two-body relaxation, dynamical friction, tidal shocks, and tidal truncation concurrently for each GC. We assume that a GC is destroyed when its mass drops below $M_{gc} = 10^4$ M$_\odot$, because of the observed scarcity of Milky Way's GCs with masses below this threshold.

5 SIMULATION RESULTS

In this section we compare the results of four different models for the star formation efficiency $\eta_i(z)$ as a function of redshift and halo mass (parameter γ). The assumed $\eta_i(z)$ as a function of redshift are shown in Figure 6.

5.1 Constant Formation Efficiency Model

In our first model we keep the formation efficiency $\eta_i(z)$ nearly constant as a function of redshift and halo mass (*i.e.*, $\gamma = 0$, $\beta = 3.5$), and we determine its value by reproducing the observed number of GCs in the Milky Way. We denote this model as the Constant Formation Efficiency model (CE).

In Figure 7 (left), we plot the cumulative distribution function (CDF) of Galactocentric distances of the GCs produced by the CE model. In this simulation, we form 145 surviving GCs, in good agreement with observations (*i.e.*, ~ 150), but this model produces more GCs at large Galactocentric distances than what is observed in the Milky Way (see the left panel of Figure 7). In addition to the Galactocentric positions, the velocity distribution of the GCs should not drastically differ from that of the Milky Way GCs or that of a similar spiral galaxy. In Figure 7 (right), we plot the CDF of the radial velocities of GCs in our simulation compared with the CDF of the radial velocities of the Milky Way and M31 GC populations and note a close agreement between our simulation and the Milky Way.

In order to improve the model, we explore which parameters in the simulations have an effect on the CDF of Galactocentric distances of the GCs. ΛCDM predicts a hierarchical merging scenario for the formation of galaxies, where the low mass haloes virialize first, followed by the more massive galaxies at a later time. In Figure 8 (top left), we plot the ages of the surviving population of GCs (assumed to be the redshift of virialization of their host halo) versus their Galactocentric distance at $z = 0$. The majority of the GCs that exist farthest from the center of the main halo formed at $2 < z < 6$. On average, the halos which produce a larger fraction of GCs which are closer to the center versus farther away tend to be the haloes which either virialized before reionization at $z \gtrsim 6$ or after the redshift of virialization of the Milky Way at $z < 2$. This result can be understood as follows. GCs that formed in haloes at $z \gtrsim 6$ belong to the most massive and rare haloes at those redshifts (because there is a minimum halo mass threshold to form a GCs system). Is well known that particles belonging to rare high-sigma peak progenitors of the Milky Way today are preferentially found near the center of the Milky Way, and so are their GCs systems (Diemand et al. 2005). At the other extreme, dwarf haloes that virialize at very low redshift tend to be rather massive and thus their orbit decays faster to the center due to dynamical friction (*e.g.*, the Magellanic clouds) and their GCs are preferentially deposited toward the halo center. In addition, GCs formed *in situ* at the redshift of virialization of the Milky Way at $z \sim 2$ are centrally concentrated, but this population is expected to have significantly higher metallicity. Indeed, the metal rich GCs tend to reside in the disk and closer to the Galactic center while the metal poor GCs are preferentially found in the halo (Zinn 1985). This supports the idea that at least a fraction of GCs closer to the Galactic center formed in more massive haloes since the metallicity of their host galaxy is proportional to the mass of the halo. Thus, we conclude that the CDF of the Galactocentric distances of GCs in our simulation and the metallicity distribution of the GC population are sensitive to the formation efficiencies as a function of redshift and halo mass. Increasing the formation efficiency

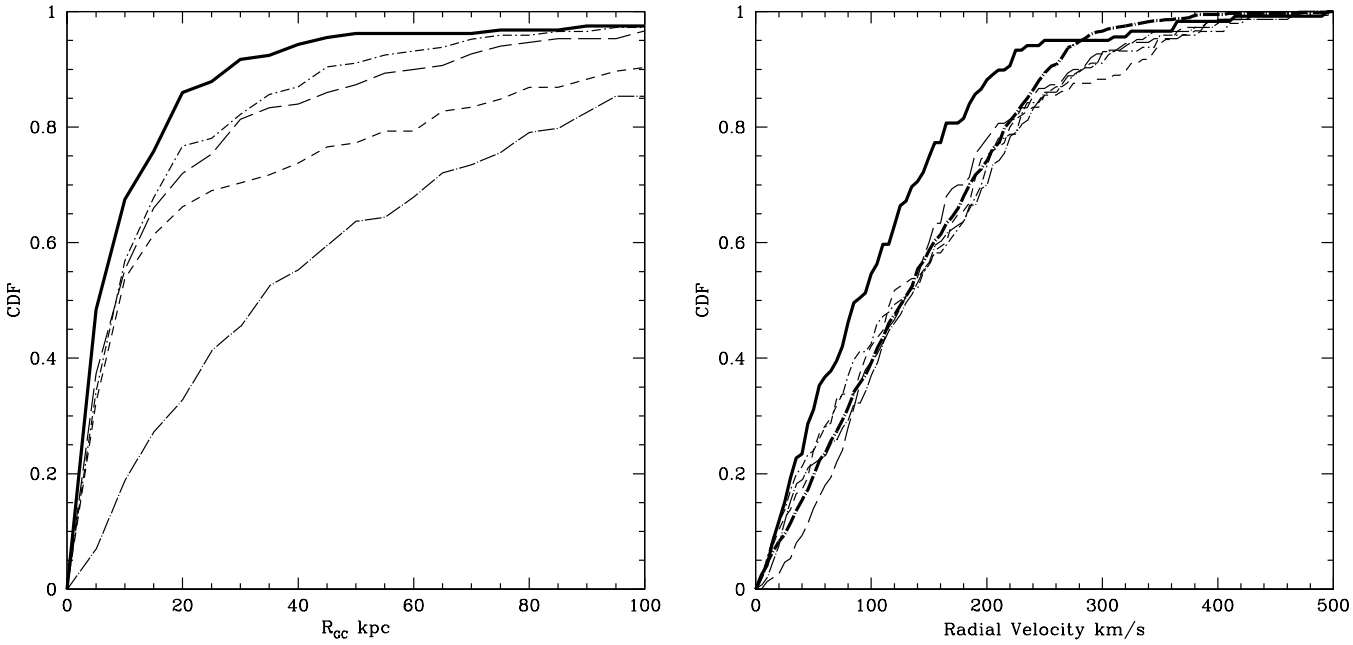

Figure 7. *Left.* The CDF of the Galactocentric distance for GCs in the Milky Way (solid), in our CE model (short dashed), in the KR13 model (long dashed), in the KR13-bis model (dot dashed). *Right.* The CDF of the radial velocities of GCs in the Milky Way (solid), in M31 (dot dashed), in our CE model (short dashed), in the KR13 model (long dashed), in the KR13-bis model (short dot dashed), in the Power Law model (long dot dashed). The positions of GCs in our model are much more sensitive to the model than the velocities.

of GCs at $z \sim 2-6$ will bias the CDF of the radial distribution of GCs in our simulation towards larger radii, whereas increasing the formation efficiency at $z < 2$ and $z > 6$ will bias this function towards smaller radii. The effect of this assumption will be explored in Section 5.2.

The GCs that are very close to the galactic center are dominated by *in situ* formation in the Milky Way progenitor. Reducing the value of β below the fiducial value $\beta = 3.5$ will reduce the fraction of *in situ* formation with respect to accreted GCs. The effect of this assumption will be explored in Section 5.3.

In the top left panel of Figure 9, we compare the GCMF produced by the CE model to the Milky Way GCMF. We see that the mass function agrees quite well with the Milky Way GCMF and note that our GCIMF is, by construction, also guaranteed to reproduce the GCMF of the local, isolated dwarf galaxies (see the right panel of Figure 3). This result is not trivial because the GCMF in the Milky Way is shaped by tidal effects in addition to two-body relaxation and stellar evolution. The response of GCs to tides is dependent on the density of the GCs which was set to reproduce the effects of two-body relaxation in isolated local dwarf galaxies. Thus, we are confident that we are capturing the relevant physical processes that determine the GCMF in the Milky Way because any attempt to resolve a possible disagreement adjusting the GCIMF or densities of GCs would break the agreement with the GCMF in isolated dwarf haloes. This is an important conclusion resulting from our self-consistent modeling of GC populations in isolated dwarfs and the Milky Way.

A summary of the parameters of the CE model is in Table 1 and the successes/failures of this model compared with observations are listed in Table 2 with KS test probability statistics in Table 3.

5.2 The KR13 Model

In order to improve the agreement of the model with the Galactocentric distribution of GCs we relax the assumption of constant GC formation efficiency that was assumed in the CE model. In this model we increase the GC formation efficiency at high redshift, before reionization, where the low mass dwarfs can survive until they reach the inner parts of the progenitor of the main halo in the simulation. Additionally, we increase the efficiency at $1.5 < z < 2.5$ where the most massive satellite haloes form their GCs. The dashed black line in Figure 6 shows $\eta_i(z)$ for this new model that we refer to as the KR13 model, due to the two humps in the formation efficiency over cosmic time. The formation efficiency in this model is also in good agreement with the constraints on the GC formation history derived from observations the galaxy luminosity functions in the Hubble deep fields (Katz & Ricotti 2013).

We produce a total of 150 GCs with this model. In Figure 7 (left), we plot the CDF of the Galactocentric distances of GCs for the KR13 model and note a much better agreement with the Milky Way than what was found for the CE model (See Table 3). The largest discrepancy between observations and the model is at Galactocentric distances between $20 < R < 60$ kpc.

As stated before, the GCMF is largely robust against changes to the formation efficiencies across cosmic time. In the bottom left panel of Figure 9, we plot the GCMF for the KR13 model and note that the peak is consistent with what

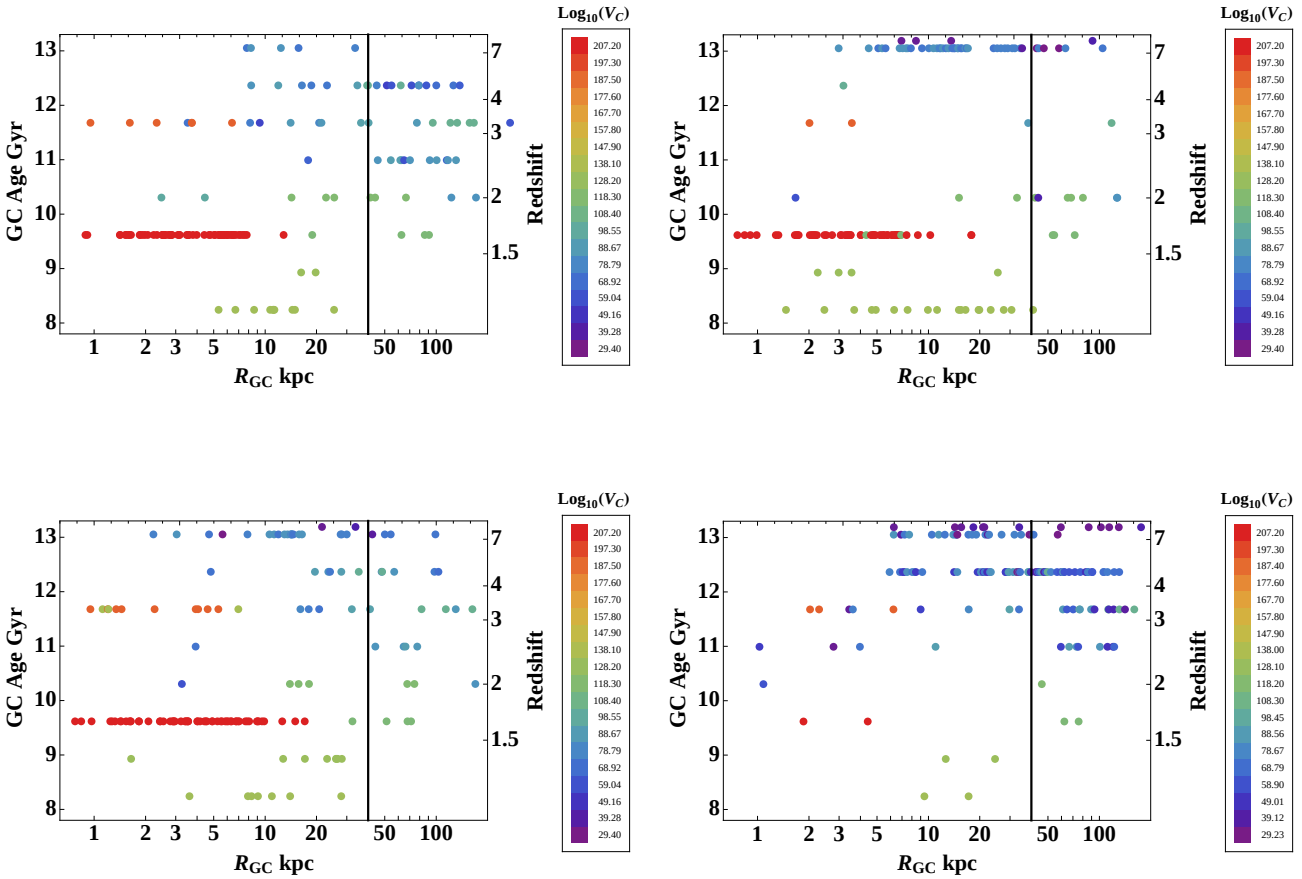

Figure 8. Galactocentric distances of the GCs versus the age in which they formed. Each individual point represents one GC and the vertical line represents the radius which ∼ 95% of the Milky Way GC population resides within. *Top Left.* CE Model. *Bottom Left.* KR13 Model. *Top Right.* KR13-bis Model. *Bottom Right.* Power Law Model

we find for the Milky Way. The radial velocities of the GCs in the KR13 model are closer to what is observed in M31 as opposed to the Milky Way. Overall the kinematics of GCs in our KR13 model are consistent with a Milky Way type spiral galaxy.

Raising the formation efficiencies above their minimum values as we have done in the KR13 model may overproduce GCs in isolated dwarf galaxies. We check to see if these formation efficiencies are consistent with observations by comparing the specific frequencies (S_N) of the few isolated dwarf galaxies in our simulation to observations. Isolated dwarfs belong to the first two classes of GCs which we described earlier, and although there are only a few isolated dwarfs because the volume of the refined region in the simulation is small, we see in Figure 11, that their specific frequencies are consistent with what is expected from the observations of Georgiev et al. (2010)[2]. A much larger volume is required to better understand the dispersion in the individual values of S_N for isolated dwarfs.

The host galaxy in which a GC forms impacts the chemical properties seen in each individual GC. The bimodal distribution of metallicities of the Milky Way GC population is likely a reflection of accreted dwarf galaxies which contributed GCs to the Milky Way as well as those GCs which formed *in situ*. Since the metallicity of a galaxy scales with its luminosity, the GCs which formed in high mass galaxies likely represent the high metallicity population while those which formed in dwarfs contribute to the lower metallicity population. The KR13 model predicts that 41% of the GC population formed *in situ* which may suggest that the Milky Way should exhibit a roughly equal split of GCs with high and low metallicity. In Figure **??**, we compare the expected metallicity distribution of the accreted GCs formed in the KR13 model[3] with the distribution of the Milky Way's GCs. Our simplistic model is used to demonstrate that the bi-

[2] Masses of the haloes were converted into luminosities using equations 13 and 14 in Georgiev et al. (2010).

[3] Metallicities are calculated by using Equations (17) and (18) from Muratov & Gnedin (2010) and assuming the intrinsic metallicity distribution of GCs in each dwarf galaxy is lower than the metallicity of the host, in a half-normal distribution with a deviation of 0.4 dex. The results are largely independent of the shape of the intrinsic metallicity spread in the case of contribution from

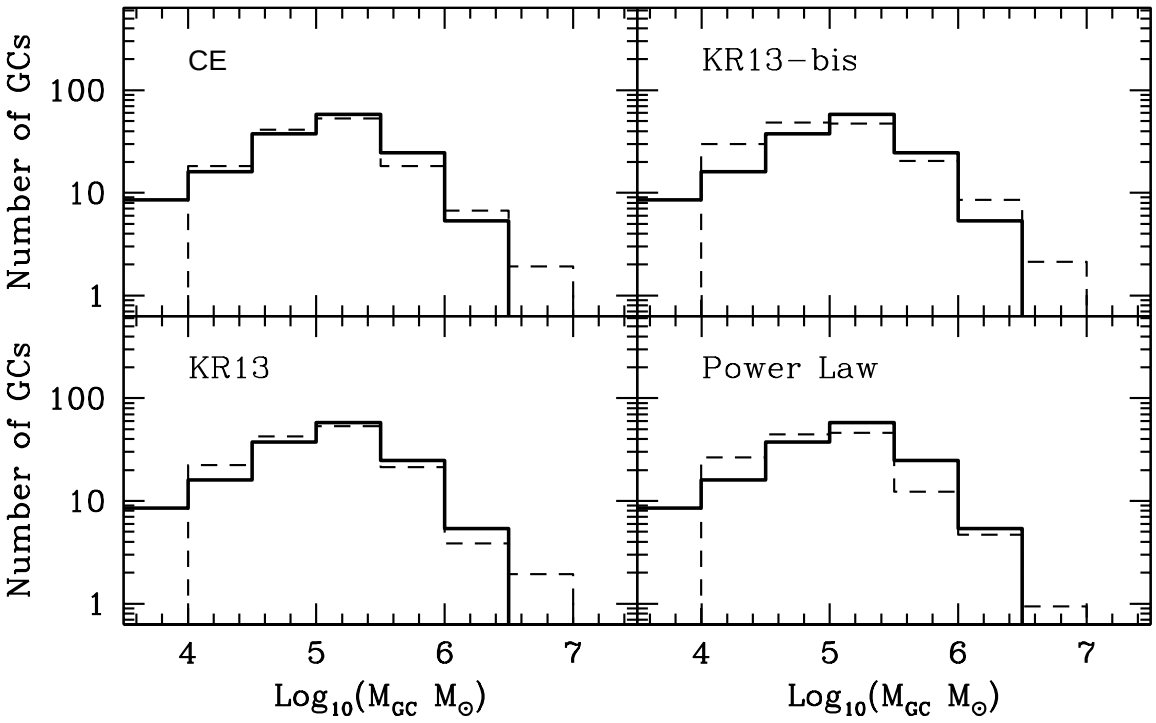

Figure 9. Mass function of GCs in each of our simulations (dashed lines) compared to that of the Milky Way (thick line). The histograms have been normalized to a population of 150 GCs. The peak of the mass function matches well for all models tested.

modal metallicity distribution of the Milky Way can be, in principle reproduced from a hierarchical merging scenario for the assumptions we have made on the intrinsic metallicity distribution. We refer the reader to Tonini (2013) where a much more in depth treatment of GC metallicities is presented within the context of the assembly of a large galaxy; however, the basic idea of an "assembly scenario" is along the lines of the methodology used in this present work which has been shown to reproduce the bimodal properties of large galaxies. Tonini (2013) conclude that the distribution of the metallicities is dependent on the assembly and star formation history of the host galaxy. It is unlikely that the assembly history of the main halo in the Via Lactea simulation exactly mimics that of the Milky Way. The present calculation is used to demonstrate that a bimodal population can be reproduced in our present framework and that it is likely also sensitive the the masses of the haloes which contribute GCs since the metallicity of the stars in a halo is partially dependent of the mass of the halo.

It is clear that this model produces significantly fewer low metallicity GCs than expected and it is unlikely that those GCs formed *in situ* can account for the deficit at low metallicities. While we have successfully reproduced the radial distribution of GCs as well as multiple other characteristics of the Milky Way GC population, this model fails to reproduce the metallicity distribution seen in the Milky Way which has a surviving population likely dominated by very old accreted GCs.

Since we have a two peaked model for the formation efficiencies, one might expect that the age distribution of the GCs in our simulation also shows this bimodal characteristic. In the top panel of Figure 10 we plot a histogram of the ages of the GCs in our simulation (solid line) and compare to those known for the Milky Way GC population (dashed line). The ages of most Milky Way GCs are only known to a precision of ±1 Gyr [but see Katz & Ricotti (2013)] and any underlying bimodality in the age distribution is smoothed out by these large uncertainties. Furthermore, our model assumes that all GCs in an individual galaxy form synchronized in an instantaneous burst, neglecting any intrinsic age spread. This simplifying assumption is reasonably realistic for dwarf galaxies (because of their short dynamical time scale) but is likely less realistic for GCs formed *in situ* in the Milky Way.

In order to test whether the ages of GCs in our simulations agree with those of the Milky Way GC population, we convolve the ages of GCs in our simulation with a Gaussian distribution with a standard deviation of 1 Gyr. Figure 13 compares the results with the observed ages of GCs in the Milky Way. We can see that simulated GCs from the KR13 model is not double peaked and appears as a continuous formation scenario consistent with what is seen for the 93 Milky Way GCs with age estimates (Forbes & Bridges 2010). There is still a overabundance of GCs forming at the time of virialization of the Milky Way, but as mentioned

many dwarf galaxies. The same is not true for the GCs formed *in situ* in the Milky Way

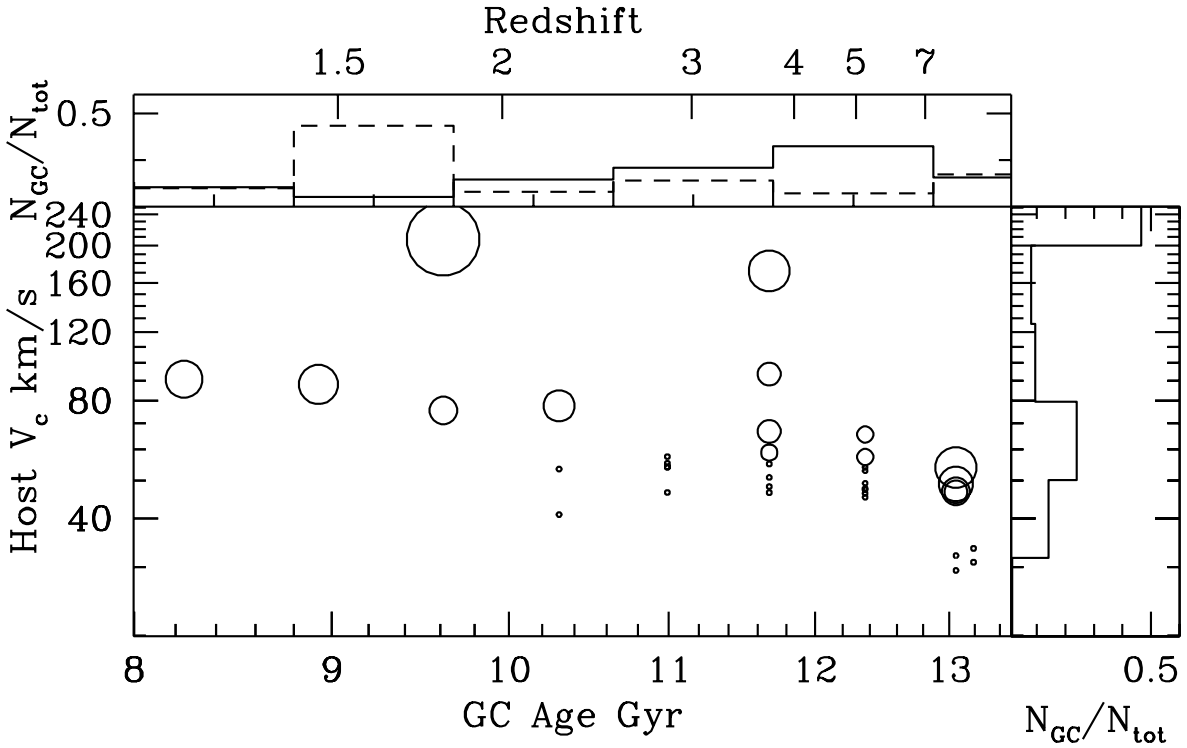

Figure 10. Formation epoch of GCs versus the circular velocity of the host halo for the KR13 model. The radius of the circle is proportional to the logarithm of the number of surviving GCs each halo contributed to the final population of the main halo. The top panel is a histogram of the ages of the GCs in the simulation (dashed line) compared to the ages of 93 of the Milky Way GCs (solid line) compiled by Forbes & Bridges (2010). The right panel is a histogram of the number of haloes of a given V_C which contributed surviving GCs. The large bubble at the top left represents the main halo in the simulation.

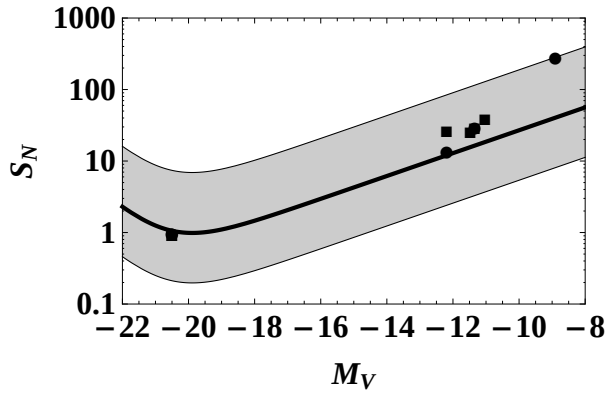

Figure 11. Specific frequency of galaxies in our simulation versus their absolute magnitude. The circles represent isolated dwarf haloes in the KR13 model, and the squares represent the isolated haloes in the KR13-bis model. The points at $M_V = -20.5$ represent the specific frequency for the main halo in our simulation which we assume to have an absolute visual magnitude equal to that of the Milky Way. The shaded region represents the expectation from Georgiev et al. (2010) with $10^{-5} < \eta < 3.5 \times 10^{-4}$. The thick black line in the middle of the shaded region represents $\eta = 5.5 \times 10^{-5}$ as derived by Georgiev et al. (2010).

before, one should convolve the GCs formed *in-situ* in the Milky Way with a larger spread for their age distribution.

A summary of the parameters of the KR13 model is in Table 1 and the model's successes/failures in matching observations can be found in Table 2 with KS test probability statistics in Table 3.

5.3 The KR13-bis Model

As previously discussed, the metallicity of GCs is likely determined by the mass of the host galaxy in which they form. A shortcoming of the KR13 model is the deficiency of low metallicity GCs with respect to observations. In order to produce more low metallicity GCs, we can increase the number of GCs formed in small mass haloes at high redshift with respect to those formed in larger mass haloes. We test a third model, the KR13-bis model where we adopt $\beta = 3$ (*i.e.*, $\gamma = -0.14$) in Equation (19) so that the model produces more GCs that formed in dwarf galaxies and were later accreted onto the Milky Way, rather than formed *in situ* in the Milky Way.

We show $\eta_i(z)$ for the KR13-bis model as the dotted line in Figure 6. We can see in the top right panel of Figure **??** that the metallicity distribution for this model is significantly improved over the KR13 model and in this model, only 38% of the total surviving GC population formed *in situ* in the Milky Way. Although the fraction that formed *in situ* is only slightly lower, we form more GCs in older lower mass halos which improves the metallicity distribution. The accreted GC population dominates the low metallicity peak but also contributes some higher metallicity GCs as also found by Muratov & Gnedin (2010). In this model number of GCs formed *in situ* in the Milky Way is roughly what is

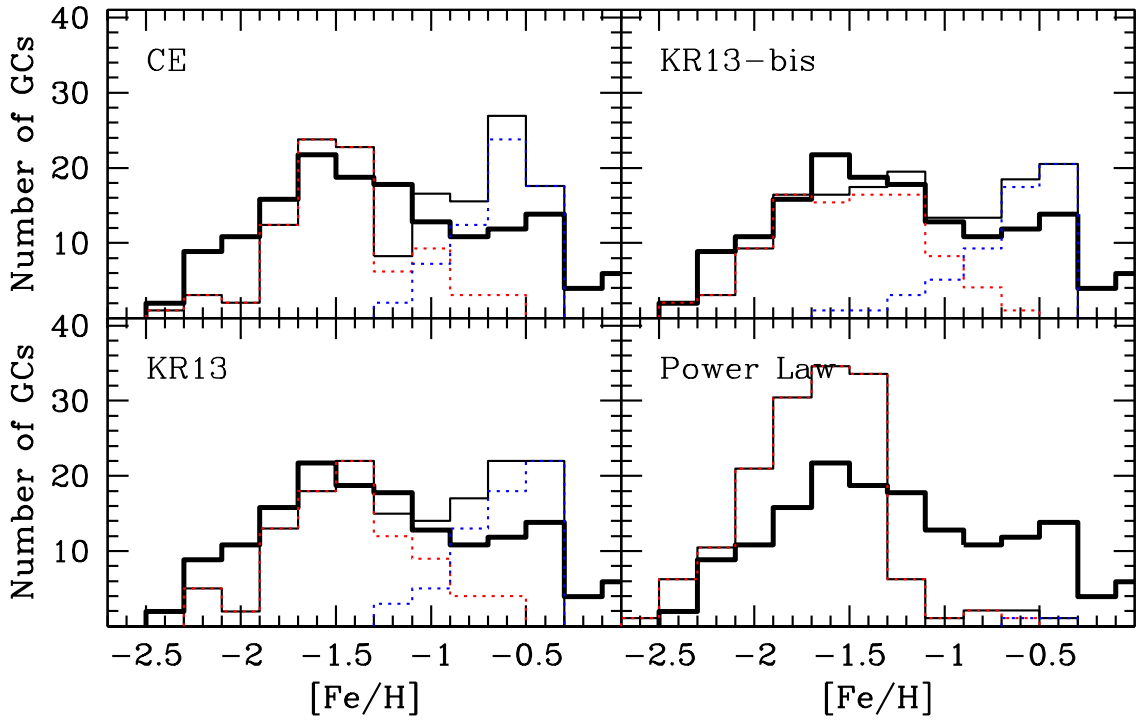

Figure 12. Metallicities of GCs in our simulations (thin line) are compared to what is observed for the Milky Way (thick line). The GCs which formed *in situ* are shown in blue and the GCs which were accreted are shown in red. $\sim 30\%$ ($\sim 60\%$) of Milky Way GCs have [Fe/H] > -1 (-1.5).

needed to fill the gap at the high metallicity end of the distribution. The GCMF produced by the KR13-bis model (see top right panel of Figure 9) remains largely unchanged from the the KR13 models and the CDF of the radial velocities is identical to that of the KR13 model and to observations of M31 (see Figure 7 (right)). Likewise, the CDF of the Galactocentric distances of the GCs is quite consistent with what is seen in the Milky Way, similarly to the KR13 model (see Figure 7 left).

Since decreasing β in Equation (19) effectively increases the formation efficiency of GCs in lower mass galaxies, a larger proportion of GCs that survive to $z = 0$ have formed earlier in low mass galaxies (see Figure 14). The most massive dwarf galaxies at high redshift contribute significantly to the total accreted GC population, accounting for about 40% of surving GCs in the Milky Way. Adopting a model with such high efficiencies may overproduce the number of GCs in isolated dwarf galaxies. In Figure 11 we compare the specific frequency of GCs in isolated dwarfs in the KR13-bis model (squares) to observations. While there are only a few isolated haloes which have GCs that have survived until the present, these few galaxies fall perfectly within the range observed in local dwarf galaxies.

A summary of the parameters of the KR13-bis model is in Table 1 and the model's successes/failures in matching observations can be found in Table 2 with KS test probability statistics in Table 3.

5.4 The Power Law Model

We test one final model where GC formation is extremely biased to occur in high redshift dwarf galaxies. We adopt a value of $\beta = 1.5$ (*i.e.*, $\gamma = -0.57$) in Equation (19) and adjust the formation efficiency as a function of redshift to a power law that is $\propto (1+z)^2$ ($\eta_i(z)$ for the Power Law model is the long dashed line in Figure 6). This model seeks to determine if the Milky Way's GC population could be formed entirely from an accreted population. Of the 143 GCs that survive within the main halo until $z = 0$, only two of these GCs were formed *in situ*.

As was observed in the three previous models, the mass function and the CDF of the GC's velocities remains largely unchanged and are consistent with what we expect for a Milky Way type galaxy. Furthermore, the ages of the GCs formed in this simulation agree well with the measured ages for the Milky Way GCs. However, we find that the CDF of the positions of the GCs drastically under predicts what is seen in the Milky Way and the GCs in this simulation are biased to much farther distances. Since we adopted such an extreme value of $\beta = 1.5$ and thus the majority of the surviving GC population was accreted from high redshift dwarf galaxies, we also find that we significantly over predict the number of low metallicity GCs in the Milky Way.

A summary of the parameters of the Power Law model is in Table 1 and the model's successes/failures in matching observations can be found in Table 2 with KS test probability statistics in Table 3.

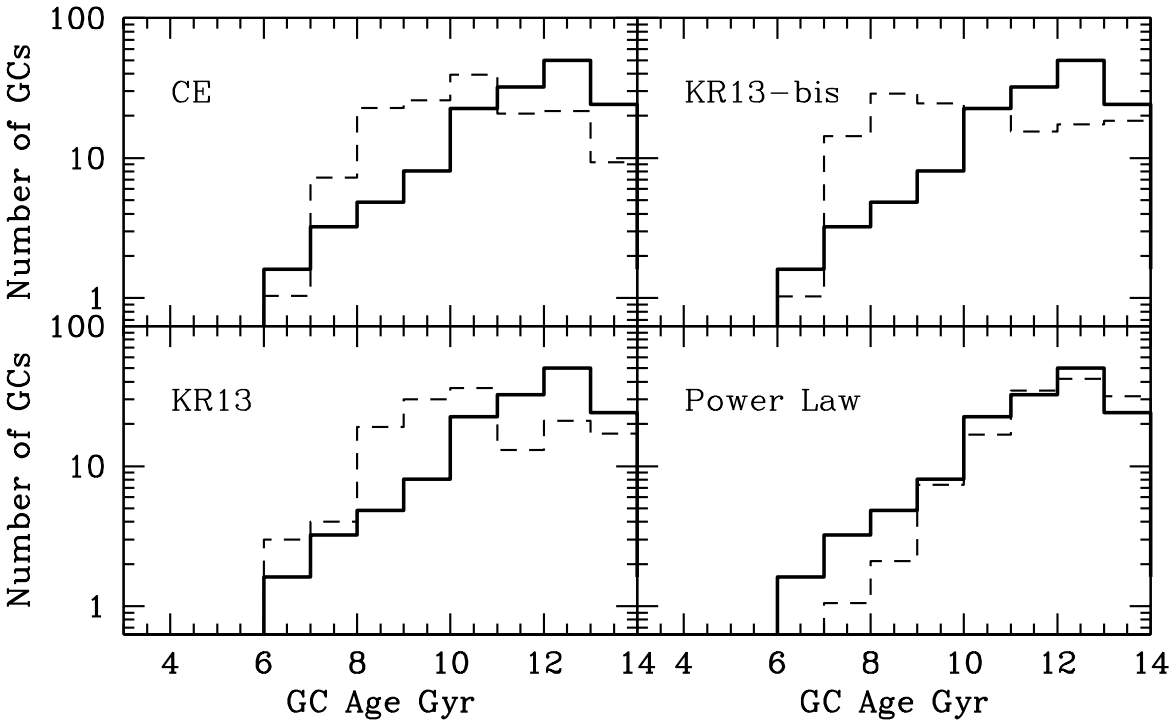

Figure 13. Ages of GCs in each of our simulations randomized over a Gaussian distribution with $\sigma = 1$ Gyr (dashed lines) compared to ages of 93 of the Milky Way GCs (solid line) compiled by Forbes & Bridges (2010). The histograms have been normalized to a population of 150 GCs.

Model	N_{GC}^{tot}	N_{GC}^{acc}	N_{GC}^{surv}	$N_{GC}^{in-situ}$	N_{Dw}^{acc}	N_{Dw}^{surv}	f_N^{surv}	f_M^{surv}	$N_{GC}(z>7)$	$f_M^{surv}(z>7)$
CE	145	335	84 (58%)	61 (42%)	63	43	27%	20%	5(3%)	10%
KR13	150	279	89 (59%)	61 (41%)	52	38	30%	19%	26(17%)	15%
KR13-bis	146	238	90 (62%)	56 (38%)	32	21	36%	20%	48(33%)	22%
Power Law	143	301	141(99%)	2 (1%)	100	70	46%	31%	36(25%)	24%

Table 1. N_{GC}^{tot} is the total number of GCs that survived to $z = 0$. N_{GC}^{acc} is the total number of accreted GCs. N_{GC}^{surv} is the number of accreted GCs that survived to $z = 0$. $N_{GC}^{in-situ}$ is the number of surviving GCs that formed *in situ*. N_{Dw}^{acc} is the number of haloes that contributed GCs to the Milky Way halo, N_{Dw}^{surv} S is the number of haloes that contributes surviving GCs to the Milky Way halo. f_N^{surv} is the percentage of GCs that survives by number and f_M^{surv} is the percentage of GCs that survive by mass. $N_{GC}(z > 7)$ and $f_M^{surv}(z > 7)$ are the total number of GCs that form at redshifts $z > 7$ and the fraction of the mass that survives from those redshifts.

6 DISCUSSION

In order to match the observed metallicity distribution function, Galactocentric distances, and ages of GCs in our models, we find that the specific (per unit dark matter halo mass) formation efficiency of GCs, $\tilde{\eta}_i$, should be bimodal with a peak at redshift $z > 6$ and should be higher in low mass haloes than in larger mass haloes.

It remains unclear whether the second peak of the formation efficiency at low redshift is a robust result of the model. For instance, a low redshift increase of the formation efficiency may be produced by GCs that may form as a result of "minor" mergers with the Milky Way after its virialization, a GC formation process that we have not modeled. However, the GC population we have designated as forming *in situ* within the Milky Way may be interpreted as a population that formed as a result of major galaxy mergers which coincide with rapid mass growth and therefore virialization of the halo. In order to reproduce the observable characteristics of the Milky Way GC population, some significant portion of GCs (about 30%) should form with the Milky Way, whether it be *in situ* or in mergers.

We can see from the left panel of Figure 7 that the positions of GCs in the Milky Way exhibit a strong radial gradient within ~ 10 kpc and our models fails to reproduce this property. From the top left panel of Figure 8 it is also clear that the majority of GCs which populate this region were formed *in situ*, within the main halo of the simulation. Unlike the accreted GCs where the initial conditions for their orbits are taken directly from the kinematics and positions of the accreted dwarf haloes, the initial conditions for the *in situ* population of GCs are relatively unconstrained. The constant density sphere which we have assumed did not reproduce the radial gradient exhibited by Milky Way GCs

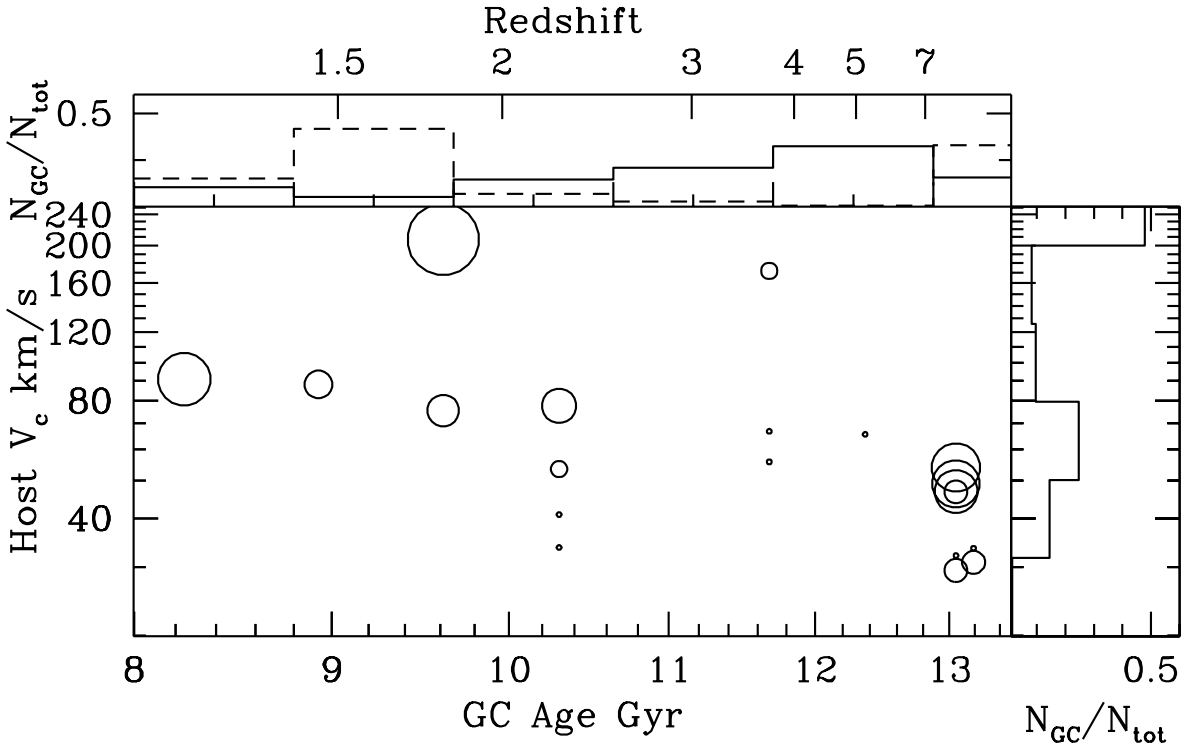

Figure 14. Formation epoch of GCs versus the circular velocity of the host halo for the KR13-bis model. The radius of the circle is proportional to the logarithm of the number of surviving GCs each halo contributed to the final population of the main halo. The top panel is a histogram of the ages of the GCs in the simulation (dashed line) compared to the ages of 93 of the Milky Way GCs (solid line) compiled by Forbes & Bridges (2010). The right panel is a histogram of the number of haloes of a given V_C which contributed surviving GCs. The large bubble at the top left represents the main halo in the simulation.

Model	GC Positions	GC Velocities	Peak Mass	Metallicity	Ages	S_N
CE	X	√	√	-	√	√
KR13	√	√	√	X	√	√
KR13-bis	√	√	√	√	√	√
Power Law	X	√	√	X	√	√

Table 2. Success of each of the three simulated models compared with observations. "√" represents a potential agreement, "X" represents a clear disagreement, and "-" means the potential agreement is unclear.

and therefore, the initial conditions we have assumed are unlikely to represent to true initial conditions of the *in situ* population. In all models (excluding the Power Law model), the population of GCs within 10 kpc is also dominated by the GCs that formed *in situ* and as we can see in left panel of Figure 7, these models are identical up to ~ 10 kpc (once again excluding the Power Law model).

The KS test probabilities for the positions will significantly improve if we choose initial conditions for the *in situ* population that reproduce this radial gradient. We would also likely have to increase the formation efficiency of the *in situ* population as more GCs will be placed closer to the center of the main halo which leads to a high probability that they will encounter the bulge. The CE models begins to diverge from the double peaked models after this fiducial radius which represents the point at which the accreted population of GCs represents the majority of the population. This suggests that the major differences between the positions in these models is due to the populations of accreted GCs and not the GCs that formed *in situ*. Since the initial conditions of the *in situ* population are not known, simply inserting a radial gradient initially, although it will improve the KS test probabilities for the positions, does not provide any additional information, as this would require testing multiple different initial conditions in order to determine which are compatible with the observed radial gradient. Given the results of our simulations, it is unlikely that the *in situ* population formed in a constant density sphere because we have failed to reproduce the radial gradient. For these reasons, we stress that the KS test probabilities for the positions should be compared between models in order to determine which model provides a better fit to the observational data.

Since we have only tested one halo, with one choice of disk and bulge parameters, it is important to understand how deviations from these parameters might effect our simulations. A more massive bulge will certainly lead to more tidal destruction as the sphere of influence will become larger. However, as we described previously, we are tightly constrained by observations on how massive our classical

Model	GC Positions	GC Velocities (MW)	GC Velocities (M31)
CE	0.11%	0.41%	30%
KR13	4.8%	0.47%	46%
KR13-bis	2.9%	0.32%	60%
Power Law	0%	0.97%	75%

Table 3. KS Test probabilities for each of the models compared with observational results.

bulge can be. Our simulations are likely much less sensitive to changes in parameters for the disk as long as it does not become so dense that it can tidally disrupt the GCs in our simulations. This is unlikely to be the case because there exists a population of GCs in the Milky Way which live close do the disk and if the disk could significantly disrupt the GCs, this population would not exist. Furthermore, disk shocking only minimally effects the GC population in our simulation and therefore, small deviations about the chosen parameters are unlikely to result is disk shocking becoming a dominant effect. The main role that changes to the disk parameters may cause is changes to the velocities of GCs. For GCs outside the disk, $V_c \propto \sqrt{M}$, and since our $z = 0$ disk mass is $\sim 70\%$ greater than the disk mass estimated by Bovy & Rix (2013), we can expect the velocities of our GCs might be $\sim 30\%$ larger than what is observed. We can see in the right panel of Figure 7 that the GCs in our simulation tend to have higher velocities than Milky Way GCs and that they tend to agree with M31 which is likely to have a more massive disk than the Milky Way. Decreasing our disk mass will almost certainly relieve some of the tension in the CDF of the velocities.

Our model makes distinct predictions for the number of GCs in the surviving population which were accreted versus formed *in situ*, within the Milky Way. We found that in order to match the observed metallicity distribution of Milky Way GCs, the majority of the surviving population (about 62%) has to form in lower mass high redshift satellite haloes. Forbes & Bridges (2010) studied 93 of the Milky Way's $\sim$ 150 GCs and provide a lower limit for the number of Milky Way GCs that were accreted and found that $27-47$ GCs ($\approx 30\%-50\%$ of the population) were accreted from $6-8$ dwarf galaxies. Our most successful model, the KR13-bis model, predicts that 62% of the Milky Way's GC population was accreted which is slightly higher than the upper limit from Forbes & Bridges (2010). Our KR13-bis simulation predicts that the present population of accreted GCs (90 GCs) comes from a total of 19 dwarfs, with 9 dwarfs each contributing less than 3 GCs (for a total of 11 GCs) and 10 contributed at least 3 surviving GCs each (for a total of 79 GCs). The number accreted dwarfs is slightly higher than the lower bound suggested by Forbes & Bridges (2010). However, looking at the metallicity distribution of GCs in the Milky Way, $\sim 30\%$ ($\sim 60\%$) of Milky Way GCs have [Fe/H] > -1 (-1.5) and the KR13-bis model predicts a reasonable number of accreted GCs, within this range, that produce the metal poor population.

Because we use only one realization of the Milky Way halo (the VL II merger tree), we are not able to capture the variance of the GC distribution due to different merger histories. We point out that even with the given merger tree, the stochasticity due to the assignment of GCs masses extracted from the GCIMF produces some fluctuations in the model results. Thus, we do not expect to reproduce exactly the Milky Way's GC population. Rather, our goal has been to understand the dominant physical processes that determine the various observables.

Despite our inability to determine the process which form GCs within the main halo, the observed ages of GCs in the Milky Way constrain the approximate epochs of formation of GCs. This allows us to make predictions for the destruction rates of GCs within the main halo. The KR13-bis model predicts a destruction rate by mass of $\sim 80\%$. We point out that this value fluctuates considerably between different runs of the same simulation but never goes below $\sim 65\%$. The destruction percentage in our simulations is very sensitive to what happens to the few 10^7 $M_\odot$ GCs in our simulation. Because we aim to form ~ 150 GCs in our model, we expect only a few of the highest mass GCs to form in the entire simulation and therefore, a large fluctuation in destruction percentage is not unexpected.

In Figure 15 we plot the number of GCs that are accreted as a function of redshift for out best fit KR13-bis model as well as the number that survived. Although 33% of GCs form in dwarf haloes at $z > 7$, we can see from the inset of Figure 15 that the bulk of all surviving GCs were accreted onto the main halo at $z < 4$ with about half having been accreted between $z = 2$ and $z = 0.7$.

We have also neglected the idea of a generic "infant mortality" of GCs where stars clusters, independent of mass, are destroyed within a few tens of Myr (Bastian et al. 2005). This destruction mechanism has no effect on our simulations ability to reproduce the observable characteristics of the Milky Way's GC population if it is independent of mass; however, this certainly may influence the role of GCs from a cosmological standpoint. Another dynamical process that we have neglected is the effect gas expulsion, suggested by Baumgardt et al. (2008), which may destroy up to 95% of all clusters within a few tens of Myr of formation. This effect is dependent on the initial mass of the cluster and tends to destroy the lower mass end of the GCIMF more effectively, thus shaping the surviving mass function. Baumgardt et al. (2008) have claimed that this destruction mechanism is nearly independent of the external tidal field and should therefore affect GCs in dwarf galaxies as well as in larger Milky Way type galaxies.

Since GCs emit the majority of their ionizing radiation within $\sim$ 10 Myr of their formation, these infant mortality mechanisms, which destroys GCs on slightly longer time scales, do not prohibit the evolution of the massive stars within GCs. Katz & Ricotti (2013) found that assuming a destruction percentage by mass of $\sim 90\%$ for GCs, if $\sim 40\%$ of GCs formed before $z \sim 6$, then they would have played a major role in the reionization of the Universe.

The destruction percentage predicted in our simulations is also sensitive to the upper and lower limits of the masses

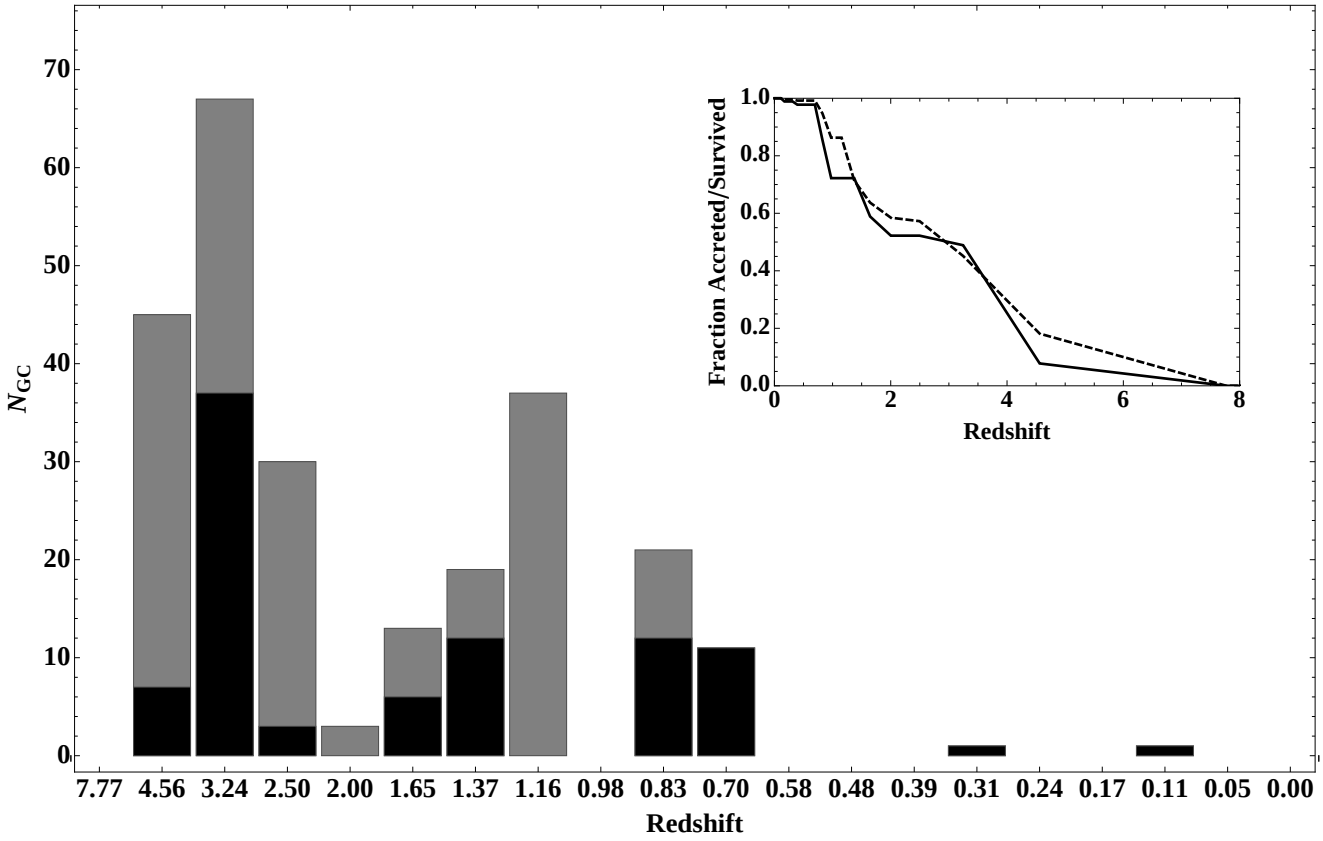

Figure 15. The grey bars represent the number of GCs that were accreted as a function of redshift while the black bars represent the number of GCs that survive. The solid line in the inset shows the CDF of the number of GCs that survived as a function of the redshift they were accreted while the dashed line represents the CDF of the number of GCs accreted as a function of redshift.

in the GCIMF. We have assumed $M_{low} = 10^5$ M$_\odot$, but if we lower this value, the destruction rate will increase roughly as given in Equation (9) (*i.e.* by a factor ~ 1.4 for $M_{low} = 10^4$ M$_\odot$), which increases the lower limit of the destruction rate by mass in our simulations from $\sim 65\%$ to $\sim 91\%$.

The destruction percentage in our simulations is further sensitive to our choice of x_{crit} which is the ratio between the half light radius and the tidal radius for which we consider our GCs destroyed. Given the density of our GCs, which was derived to match the mass function of GCs in dwarf galaxies, this destruction mechanism is only relevant in the very inner parts of the galaxy; however, since many of the GCs fall in on radial orbits, many GCs have at least one passage close to the center over their many Gyr lifetimes. Observations of the Milky Way population do not show any GCs residing within a few hundred parsecs of the galactic center where this process is effective.

We tested the effects of turning this process off for the KR13-bis model and found that, despite producing many more GCs and found a destruction percentage by mass of $\sim 50\%$ compared to the previous 80%. However, the velocity distribution, mass function, and ratio between the number of GCs formed *in situ* versus accreted which survive also remained the same which gives the right metallicity distribution and ages. The positions of GCs in the simulation compared to the Milky Way slightly improve because more GCs are allowed to remain at the center. This suggests that if we renormalize the efficiency as a function of redshift to produce the correct number of GCs, all aspects of the KR13-bis model which reproduce observations of the Milky Way GC population will once again be reproduced with a smaller destruction percentage. Thus we emphasize that the choice of normalization for the efficiency of forming GCs as a function of redshift is degenerate with this destruction mechanism as well as our choice of lower limit on mass in addition to any assumption we make for infant mortality. We are constrained to not overproduce or underproduce GCs in isolated dwarf galaxies and since our choice of x_{crit} is slightly low, the fact that we reproduce the populations of GCs in isolated dwarfs suggests that our choice of normalization, although degenerate with many parameters, is reasonable since our choice of x_{crit} does not effect the populations of GCs in the isolated dwarfs. To conclude this point, the shape of the efficiency curve as a function of redshift produces the correct positions, mass function, velocity distribution, metallicity distribution and age distribution and this property is entirely robust to changes in the normalization of the curve.

7 DID GLOBULAR CLUSTERS REIONIZE THE UNIVERSE?

Using the constraints from our simulations, we can determine the role that GCs may have played in the reionization

of the Universe. Ricotti (2002) demonstrated that the expected number of ionizing photons per baryon by GCs per Hubble time at redshift 7 is:

$$N_{ph}^{gc} = f_{esc}\eta\omega_{gc}\frac{t_H(z=7)}{\Delta t_{gc}}. \quad (23)$$

where $f_{esc} \sim 1$ is the escape fraction of photons from GCs (see Ricotti (2002) for discussion of this value), $\eta = 8967$ is the number of ionizing photons per baryon in stars which is constrained from STARBURST99 (Leitherer et al. 1999) which can certainly increase with a more top-heavy stellar IMF as discussed in Schaerer & Charbonnel (2011), $t_H(z = 7)$ is the Hubble time at $z = 7$, $\omega_{gc} \approx 2.1 f_{di}(2.7^{+2.3}_{-1.7} \times 10^{-4})$ is the fraction of cosmic baryons converted into stars, Δt_{gc} is the time period over which GCs form, and f_{di} is the inverse of the survival percentage by mass. From Table 1, we know that in the KR13-bis model predicts $f_{di} \approx 4.55$ during the reionization epoch. Furthermore, the value of $t_H(z = 7)/\Delta t_{gc}$ effectively sets the fraction of GCs which form prior to the epoch of reionization, f_{ri}, which is found in our KR13-bis model to be $f_{ri} = 29\%$. We can, therefore, rewrite the previous equation as follows:

$$N_{ph}^{gc} = 5.08 f_{ri} f_{di} = 6.7 \quad (24)$$

As previously discussed, our simulations likely predict the correct shape of η_i as a function of redshift, but the normalization is slightly less constrained. We can perform the same calculation to predict the role GCs may have played in the reionization of the Universe by substituting the ω_{gc} as derived by Ricotti (2002) with the one found empirically within our simulation.

In the KR13-bis model, 122 GCs formed in the system at $z > 7$, and thus, on average, the total mass in GCs during the reionization epoch is $M_{gc}(z > 7) = N_{gc}(z > 7)\langle m_{gc}\rangle^{ini} = 6.34 \times 10^7$ M$_\odot$. Thus, $\omega_{gc} f_{ri} = M_{gc}(z > 7)/(M_{MW}\Omega_b/\Omega_{dm}) = 4.11 \times 10^{-4}$ and we determine M_{MW} using Equation 18 with the maximum circular velocity of the main halo. Using this value along with Ω_{DM}/Ω_b from Planck Collaboration et al. (2013), we determine that $N_{ph}^{gc} = 4.04$. Despite this more conservative value, this calculation also yields a value of N_{ph}^{gc} that is in reasonable agreement with the previous calculation.

The number of ionizing photons per baryon per Hubble time N_{ph}^{gc} needed to reionize and maintain the ionization of the IGM at redshift z is $N_{ph}^{gc} = 1 + t_H/t_{rec}$, where t_{rec} is the hydrogen recombination time. If we define a clumping factor of the IGM $C \equiv \langle n^2\rangle/\langle n\rangle^2$, we find

$$t_H/t_{rec} \approx 0.68C\left(\frac{1+z}{8}\right)^{1.5}. \quad (25)$$

Thus, assuming $C = 2.11$ as found in recent simulations (Shull et al. 2012), we need $N_{ph}^{gc} = 2.43$ ionizing photons escaping galaxies to keep the IGM ionized at $z = 7$. Our estimate of $N_{ph}^{gc} = 6.7$ from GCs at $z = 7$ implies that if $f_{esc} > 36\%$, radiation from GCs alone is sufficient for reionization. We also point out that our estimate of N_{ph}^{gc} is rather conservative because we have assumed $M_{gc}^{min} = 10^5$ M$_\odot$, a Kroupa IMF and have neglected infant mortality of clusters. For instance, as discussed in the previous section, $M_{gc}^{min} = 10^4$ M$_\odot$ would produce 1.4 times more photons, thus with this assumption, $f_{esc} = 26\%$ would be sufficient for reionization.

The value of f_{esc} for GCs is not well constrained. It depends strongly on the formation model of GCs, in particular, whether or not they form deeply embedded in much more massive molecular clouds. However, a large efficiency of conversion of gas into stars is required by models GCs formation to avoid unbinding the cluster as a result of gas loss due to stellar feedback. A high star formation efficiency has the twofold effect of increasing the feedback energy and the number of photons emitted with respect to the number of absorbing neutral atoms in the unused gas. For this reason, and because GCs are typically found in the outskirts of dwarf galaxies where the gas density is expected to be low, values of $f_{esc} \sim 0.5 - 1$ are not unreasonable. But regardless of its value, f_{esc} for GCs should be larger when compared to other modes of star formation.

8 CONCLUSIONS

We have self consistently modeled the formation history and dynamical evolution of the GC population of a Milky Way type galaxy by constraining the GCIMF and formation efficiencies to match observations of GC populations in local, isolated dwarf galaxies (Georgiev et al. 2010).

We have used the merger tree from the Via Lactea II simulation and GC orbits are computed in a time varying gravitational potential after they are either accreted from a satellite halo or formed *in situ*, within the Milky Way halo. Stellar evolution, two-body relaxation, dynamical friction, tidal shocks, and tidal truncation are calculated for each individual cluster in order to reproduce the observed kinematics and mass function of the observed Milky Way GC population.

We find that the Galactocentric distances of GCs in our simulations are very sensitive to the formation efficiencies of GCs as a function of redshift and halo mass. Our most accurate model reproduces the Galactocentric positions, velocities, mass function, metallicity, and age distributions of GCs in the Milky Way, while being consistent with the specific frequency S_N of GCs in isolated dwarf galaxies. This model predicts that $\sim 38\%$ of the surviving GCs were formed *in situ* while the other $\sim 62\%$ were accreted from about 20 satellite dwarf galaxies with $v_{cir} > 30$ km/s.

Since we have not tested all possible models for the formation efficiency as a function of redshift and halo mass as well as any other parameter one might conclude the formation efficiency may depend on, we cannot say that the double peaked model is the only way to reproduce the observations in the Milky Way. However, this model provides a natural explanation for the observable properties of the Milky Way and local dwarf GC populations while also conforming to the constraints on when GCs can form as outlined by Katz & Ricotti (2013). For these reasons, our model provides a very likely scenario for the formation and evolution of GCs in hierarchical cosmology.

Our most accurate models reveals two distinct peaks in the GC formation efficiency at $z \sim 2$ and $z \sim 7 - 12$ and a GC formation efficiency that is either remains constant or increases with decreasing halo mass, contrary $f_* \equiv M_*/M_h$ in present day galaxies that instead declines rather steeply with decreasing halo.

Thus, we expect that GC formation was likely a dom-

inant mode of star formation at least in a subset of dwarf galaxies at high-redshift whose remnants in the present day universe can be identified as early type dwarf galaxies. This trend with halo mass combined with evidence of a peaking GC's formation efficiency at redshifts $z > 6$ found in this work as well as by Katz & Ricotti (2013), using a completely independent method, supports the notion that GCs may have played a dominant role in the reionization of the intergalactic medium (Ricotti 2002).

ACKNOWLEDGMENTS

We thank the anonymous referee for revising and improving the manuscript. We also acknowledge Nate Bastian for his very helpful comments and suggestions. HK's research is supported by Foundation Boustany, Cambridge Overseas Trust, and the Isaac Newton Studentship. MR's research is supported by NASA grant NNX10AH10G and NSF CMMI1125285. This work made in the ILP LABEX (under reference ANR-10-LABX-63) was supported by French state funds managed by the ANR within the Investissements d'Avenir programme under reference ANR-11-IDEX-0004-02.

REFERENCES

Angus G. W., Diaferio A., 2009, MNRAS, 396, 887
Bastian N., Gieles M., Lamers H. J. G. L. M., Scheepmaker R. A., de Grijs R., 2005, A&A, 431, 905
Baumgardt H., 1998, A&A, 330, 480
Baumgardt H., Kroupa P., Parmentier G., 2008, MNRAS, 384, 1231
Binney J., Tremaine S., 1987, Galactic dynamics
Blakeslee J. P., 1999, AJ, 118, 1506
Bovy J., Rix H.-W., 2013, ApJ, 779, 115
Carretta E., Bragaglia A., Gratton R., D'Orazi V., Lucatello S., 2009, A&A, 508, 695
Chandrasekhar S., 1943, ApJ, 97, 255
Diemand J., Kuhlen M., Madau P., Zemp M., Moore B., Potter D., Stadel J., 2008, Nature, 454, 735
Diemand J., Madau P., Moore B., 2005, MNRAS, 364, 367
Dotter A., Sarajedini A., Anderson J., 2011, ApJ, 738, 74
Faifer F. R. et al., 2011, MNRAS, 416, 155
Fall S. M., Zhang Q., 2001, ApJ, 561, 751
Forbes D. A., Bridges T., 2010, MNRAS, 404, 1203
Galleti S., Federici L., Bellazzini M., Fusi Pecci F., Macrina S., 2004, A&A, 416, 917
Georgiev I. Y., Hilker M., Puzia T. H., Goudfrooij P., Baumgardt H., 2009a, MNRAS, 396, 1075
Georgiev I. Y., Puzia T. H., Goudfrooij P., Hilker M., 2010, MNRAS, 406, 1967
Georgiev I. Y., Puzia T. H., Hilker M., Goudfrooij P., 2009b, MNRAS, 392, 879
Gnedin O. Y., Ostriker J. P., 1997, ApJ, 474, 223
Goerdt T., Moore B., Read J. I., Stadel J., Zemp M., 2006, MNRAS, 368, 1073
Griffen B. F., Drinkwater M. J., Thomas P. A., Helly J. C., Pimbblet K. A., 2010, MNRAS, 405, 375
Harris W. E., 1996, AJ, 112, 1487
Hénon M., 1961, Annales d'Astrophysique, 24, 369
Inoue S., 2009, MNRAS, 397, 709
Irrgang A., Wilcox B., Tucker E., Schiefelbein L., 2013, A&A, 549, A137
James G., François P., Bonifacio P., Carretta E., Gratton R. G., Spite F., 2004, A&A, 427, 825
Katz H., Ricotti M., 2013, MNRAS, 432, 3250
Klypin A., Zhao H., Somerville R. S., 2002, ApJ, 573, 597
Kravtsov A. V., Gnedin O. Y., 2005, ApJ, 623, 650
Kroupa P., 2001, MNRAS, 322, 231
Leitherer C. et al., 1999, ApJS, 123, 3
Marín-Franch A. et al., 2009, ApJ, 694, 1498
Miyamoto M., Nagai R., 1975, PASJ, 27, 533
Muratov A. L., Gnedin O. Y., 2010, ApJ, 718, 1266
Ochsenbein F., Bauer P., Marcout J., 2000, A&AS, 143, 23
Ostriker J. P., Gnedin O. Y., 1997, ApJ, 487, 667
Paczynski B., 1990, ApJ, 348, 485
Peacock M. B., Maccarone T. J., Knigge C., Kundu A., Waters C. Z., Zepf S. E., Zurek D. R., 2010, MNRAS, 402, 803
Planck Collaboration et al., 2013, ArXiv e-prints
Plummer H. C., 1911, MNRAS, 71, 460
Pota V. et al., 2013, MNRAS, 428, 389
Prieto J. L., Gnedin O. Y., 2008, ApJ, 689, 919
Read J. I., Goerdt T., Moore B., Pontzen A. P., Stadel J., Lake G., 2006, MNRAS, 373, 1451
Ricotti M., 2002, MNRAS, 336, L33
Rosenberg A., Saviane I., Piotto G., Aparicio A., 1999, AJ, 118, 2306
Salaris M., Weiss A., 2002, A&A, 388, 492
Sánchez-Salcedo F. J., Reyes-Iturbide J., Hernandez X., 2006, MNRAS, 370, 1829
Schaerer D., Charbonnel C., 2011, MNRAS, 413, 2297
Schuberth Y., Richtler T., Hilker M., Dirsch B., Bassino L. P., Romanowsky A. J., Infante L., 2010, A&A, 513, A52
Shen J., Rich R. M., Kormendy J., Howard C. D., De Propris R., Kunder A., 2010, ApJ, 720, L72
Shull J. M., Harness A., Trenti M., Smith B. D., 2012, ApJ, 747, 100
Sneden C., 2005, Highlights of Astronomy, 13, 149
Spergel D. N. et al., 2007, ApJS, 170, 377
Spitler L. R., Forbes D. A., 2009, MNRAS, 392, L1
Spitzer L., 1987, Dynamical evolution of globular clusters
Strader J. et al., 2011, ApJS, 197, 33
Tonini C., 2013, ApJ, 762, 39
VandenBerg D. A., Brogaard K., Leaman R., Casagrande L., 2013, ApJ, 775, 134
Zepf S. E., Ashman K. M., 1993, MNRAS, 264, 611
Zinn R., 1985, ApJ, 293, 424
Zinnecker H., Piskunov A. E., Kharchenko N. V., Röser S., Schilbach E., Scholz R.-D., 2009, in IAU Symposium, Vol. 254, IAU Symposium, Andersen J., Nordströara, m B., Bland-Hawthorn J., eds., pp. 221–226

APPENDIX A: RELAXING THE APPROXIMATION OF CONSTANT INITIAL DENSITY OF GCS

We have assumed that all GCs, regardless of mass have constant density (hereafter, we refer to this model as UD [universal density] model). We keep the assumption that GCs maintain a constant density as they evolve, but we explore

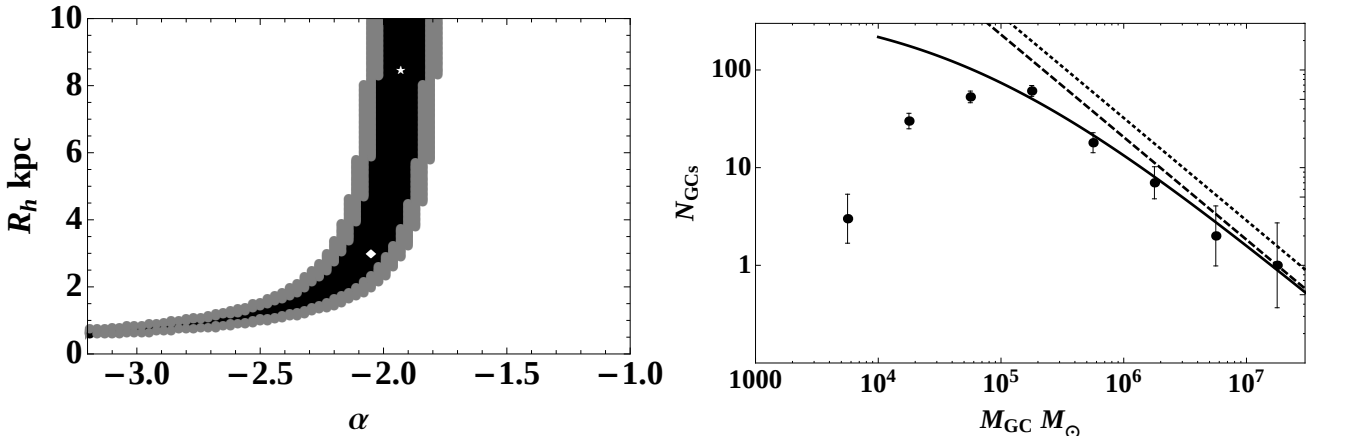

Figure A1. *Left.* Parameter space analysis of the best fit slope and initial half mass radius for the GCIMF for the UIRM. The star is the best fit parameters and the black and gray regions are the 1σ and 2σ confidence levels respectively. The diamond represents the actual parameters we have adopted so the initial R_h is much closer to that of the Milky Way GCs. *Right.* Our chosen GCIMF parameters compared with the dwarf galaxy GCMF for the UIRM. Data points represent the local dwarf galaxy GCMF from Georgiev et al. (2009b,a). The dotted line is the GCIMF prior to stellar evolution. The dashed black like is the GCMF after stellar evolution and the solid black line is the GCMF after undergoing two-body relaxation for 12 Gyr

the case in which the initial density of each GC is related to their mass. To test this idea, we assume that all GCs have a constant R_h so that $\rho_h \propto M_{gc}$ (universal initial radius [UIR] model). We run a similar parameter space exploration as was done for the UD model by leaving the initial R_h and α as free parameters; however we only compare to the high mass end of the local dwarf galaxy GCMF where tidal effects are negligible. The left panel of Figure A1 shows the results of this simulation. The current average R_h for Milky Way GCs is 2.4 pc. Once again assuming that 30% of the mass is initially lost due to stellar evolution, if the GCs remain at the same density, the minimum necessary R_h is ~ 2.7 pc. The initial R_h is likely larger since there are other effects that remove mass from the GC. If we choose the same slope of $\alpha = -2.05$ for the GCIMF and set $R_h = 3$ pc at formation and evolve this GCIMF via stellar evolution and two-body relaxation, we find that the resulting GCMF is no longer consistent with the mass function of local dwarf GCs (see the right panel of Figure A1). The data after the peak fits as well as when we assumed that all GCs had the same density regardless of mass. Tidal effects may begin to play a role towards the lower end of the mass spectrum which will likely change the shape. In this scenario, a 10^4 $M_\odot$ GC will have $\rho_h = 88.4$ $M_\odot/pc^3$, which is over an order of magnitude lower than the previous model.

The dwarf galaxy GC mass function can also reveal the maximum mass GC that can form. In this sample, the maximum mass GC has a mass of 1.07×10^7 $M_\odot$ and thus our GCIMF is require to produce GCs of at least this mass. We choose a maximum mass of 2.9×10^7 $M_\odot$, but note that the probability of producing an object of this size is minimal. Our simulations are much less sensitive to the upper bound of the mass function compared to the lower bound so any reasonable deviation to the upper bound will produce similar results.

For the UIR model we find an average KS probability of 2.7% with a maximum probability of 3.8% which is clearly lower than what was found for the UD model. Either the UD model better represents the actual initial properties of GCs in dwarf galaxies or the tidal effects which we have not included are very important. Prieto & Gnedin (2008) have run models similar to the UIRM and found that the resulting mass function is inconsistent with that of the Milky Way.

While it remains difficult to prove the exact shape of the GCIMF, whether it be a power law, Gaussian, or some other function, all shapes will look very similar towards the high mass end and have a slope approaching $\alpha = -2$. It may be reasonable to look to the open cluster mass function and compare with GC. Surprisingly, the high mass open clusters also have a power law IMF with a slope of $\alpha = -2$ which is reasonably consistent with what we have found for GCs (Zinnecker et al. 2009).

APPENDIX B: MINIMUM FORMATION EFFICIENCIES

Implementing the the minimum formation efficiencies derived in Section 3.2, for both red and blue galaxies, into our simulations is not straight forward, due to our inability to differentiate between these two types of galaxies in our simulation. For this reason, we take an alternative approach to determine an alternative set of formation efficiencies, independent of the type of galaxy. We will find that we can accurately reproduce the mean number of galaxies that should contain at least one GC as a function of absolute magnitude, consistent with the observations of Georgiev et al. (2010).

We can define the average mass of a GC from our GCIMF as follows:

$$m_{avg} = \frac{\int_{M_{low}}^{M_{up}} M' \times M'^{\alpha} dM'}{\int_{M_{low}}^{M_{up}} M'^{\alpha} dM'}. \quad \text{(B1)}$$

The cumulative distribution function (CDF) of the GCIMF

can be calculated by:

$$CDF(M) = \frac{\int_{M_{low}}^{M} M'^{\alpha} dM'}{\int_{M_{low}}^{M_{up}} M'^{\alpha} dM'}. \quad \text{(B2)}$$

If we integrate the derivative of the CDF from the minimum mass needed to survive two-body relaxation and stellar evolution, M_{surv}, up to the upper bound of the GCIMF, we can find the probability of drawing a GC from the GCIMF that will survive a specific amount of time. The probability of survival is defined as:

$$P(M_{surv}) = \int_{M_{surv}}^{M_{up}} \frac{\partial CDF(M)}{\partial M} dM. \quad \text{(B3)}$$

Since their are roughly 50 galaxies in Figure 4 in Georgiev et al. (2010) with absolute visual magnitudes brighter than -16.5, the magnitude at which nearly all galaxies brighter have at least one observed GC, the probability that randomly sampling from our GCIMF results in a galaxy of this brightness having no GCs with a mass greater than M_{surv} must be less than $\sim 1/50$ or $\sim 2\%$. The number of GCs needed to assure that a galaxy has at least one GC with a mass greater than M_{surv} is then:

$$N_{GCs} = \lceil \frac{\log(1/50)}{\log(1 - P(M_{surv}))} \rceil \quad \text{(B4)}$$

where $\lceil x \rceil$ is the ceiling function. Thus if we assign N_{GCs} to a galaxy, there is only a $\sim 2\%$ probability that stellar evolution and two-body relaxation alone will destroy all the GCs in that galaxy.

The specific formation efficiency of old GCs, η, describes the relation between the the mass of the host halo and the mass of GCs and is heavily constrained by observations. Assuming that the mass in GCs is proportional to the mass of the host halo:

$$M_{GCs} = \eta M_h \quad \text{(B5)}$$

Using Equations (13) and (14) from Georgiev et al. (2010), and the halo mass of $M_{h,-16.5}$ (which corresponds to an $M_V = -16.5$) such that all galaxies with mass greater than $M_{h,-16.5}$, have at least one GC, we can calculate η directly by knowing a value of N_{GCs} as follows:

$$\eta \approx \frac{P(M_{surv}) N_{GCs} (0.7 m_{surv} - m_{2br})}{M_{h,fid}} \quad \text{(B6)}$$

where m_{2br} is the mass loss due to two-body relaxation, the 0.7 is a result of assuming 30% of the mass is initially lost to stellar evolution, and m_{surv} is the average mass of a GC in the GCIMF with masses greater than M_{surv}.

$$m_{surv} = \frac{\int_{M_{surv}}^{M_{up}} M' \times M'^{\alpha} dM'}{\int_{M_{surv}}^{M_{up}} M'^{\alpha} dM'} \quad \text{(B7)}$$

The value of η_i can also be calculated by:

$$\eta_i = \frac{N_{GCs} m_{avg}}{M_{h,fid}} \quad \text{(B8)}$$

This derivation is clearly independent of the type of galaxy and we can see, in Figure B1, that we have once again reproduced the mean number of galaxies expected to host at least one GC as a function of absolute visual magnitude.

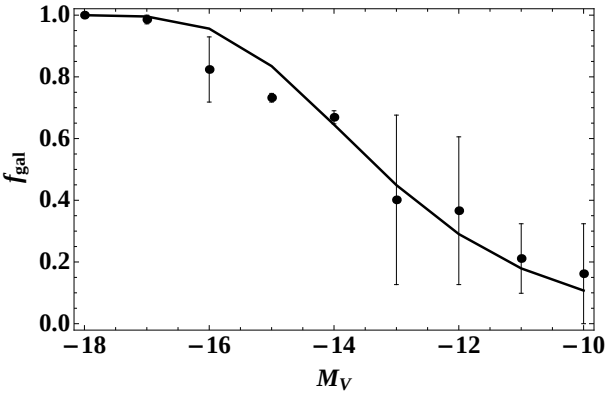

Figure B1. The percentage of galaxies expected to host at least one GC as a function of the absolute visual magnitude of the host galaxy. The solid line is the expectation using the efficiency for GC mass loss after 12 Gyr and the data points are the average of the blue and red galaxies that host at least one GC from Georgiev et al. (2010). Error bars on data points correspond to the range between red and blue galaxies and the true dispersion in the mean of all galaxies is likely larger than what is plotted.